Performance Analysis of Intelligent and Surface-Enabled Wireless Networks

Zhandos Zhakipov, B. Eng in Electrical and Computer Engineering

Submitted in fulfilment of the requirements
for the degree of Master of Science
in Electrical and Computer Engineering

School of Engineering and Digital Sciences
Department of Electrical and Computer Engineering
Nazarbayev University

53 Kabanbay Batyr Avenue,
Astana, Kazakhstan, 010000

Supervisor: Dr. Galymzhan Nauryzbayev

March 2024

Declaration

I hereby, declare that this manuscript, entitled "*Performance Analysis of Intelligent and Surface-Enabled Wireless Networks*", is the result of my own work except for quotations and citations which have been duly acknowledged.

I also declare that, to the best of my knowledge and belief, it has not been previously or concurrently submitted, in whole or in part, for any other degree or diploma at Nazarbayev University or any other national or international institution.

(signature of author)

_ _ _ _ _ _ _ _ _ _ _ _ _ _ _

Name: Zhandos Zhakipov

Date: 5 April 2024

Abstract

One of the technologies that will allow 6G to function is reconfigurable intelligent surface (RIS), which was the focus of this master's thesis. The article provided a thorough analysis of RIS, including its design, operation, and features. The RIS-aided system's performance was assessed using two system models, namely cascaded RISs-aided system and RIS partitioning system. The current state of the art in research was outlined and research gaps were identified for this system models. For both models, closed-form probability distribution functions (PDFs) were derived and validated by using Monte-Carlo simulations. For the cascaded RIS-aided systems, analytical approximation errors were validated by the Kolmogorov-Smirnov goodness-of-fit-test. Based on the results of the system assessment, it was found that the outage probability (OP) metric drops as the number of RISs in series grows. This is because more RISs mean more path-loss in the system, which means more power is needed. An improvement in the OP metric is seen when other system parameters, such as diversity path parameter (m), average received power parameter (Ω), and number of reflecting elements per RIS (N), are increased. A longer route for the signal to go to the user, and thus greater power received at the destination, is represented by an increase in the m parameter. A higher value for the received average power, as measured by the average power parameter, indicates a better operation metric. An interesting finding is that the received power doubles by 8 dBm for every doubling increase of N, which is the number of reflecting components. Analytical and simulational data are provided for each of these findings. All of the results had their approximation errors computed, and the KS goodness-of-fit test confirmed them. The RIS partitioning network is the following system model. Analytical and experimental studies were conducted on this system. We obtained closed-form PDF for the analytical findings. The Monte-Carlo simulation confirmed the closed-form equation. The results of the experiments show that RIS partitioning is effective and offers several benefits. There is a 6 dBm

improvement in received power for near-field communication when both non-orthogonal-multiple-access (NOMA) users are in the same location. Since each element of the RIS is dedicated to serving just one user, the received power remains same even when NOMA users are located in various locations. When comparing far-field communication employing all RIS components to half-RIS, the difference in received power was just -5 dBm.

Acknowledgements

I would like to express my deep gratitude to my supervisor, Dr. Galymzhan Nauryzbayev, for his guidance and support throughout the research process. I would also like to thank Dr. Sultangali Arzykulov, who has provided me with valuable knowledge related to my topic. Their feedback and support allowed me to overcome the difficulties I faced during the research process.

Finally, I would like to thank my family for their endless support throughout this time. Eventually, I was able to finish my research thanks to my surroundings.

Table of Contents

Declaration 1
Abstract 2
Acknowledgements 4
List of Abbreviations 6
List of Figures 7
List of Tables 8
Chapter 1 – Introduction 9
1.1 Background 9
1.2 Fundamental Principles of RIS 10
1.2.1 Hardware Architecture of RIS 11
1.2.2 Main challenges in designing and implementing RIS 12
1.2.3 Applications of RIS 14
1.3 Aims and Objectives 16
1.4 Literature Review 17
Chapter 2 – Methodology 22
2.1 Cascaded RISs-aided system 22
2.3 RIS Partitioning System 28
2.3.1 Analytical Approach 28
2.3.2 Experimental Approach 30
Chapter 3 – Results & Discussions 35
3.1.1 KS goodness-of-fit test 36
3.1.2 Performance analysis 37
3.2 RIS-partitioning system 42
3.2.1 Analytical approach 42
3.2.2 Experimental Approach 44
Chapter 4 – Conclusion 51
List of Publication 53
Bibliography 54

List of Abbreviations

5G	Fifth Generation
6G	Sixth Generation
AWGN	Additive White Gaussian Noise
BS	Base Station
CSI	Channel state information
IoT	Internet of Things
KS	Kolmogorov-Smirnov
LoS	Line-of-sight
MIMO	Mulitple-input multiple-output
MISO	Multiple-input single-output
MMM	Moment Matching Method
NOMA	Non-Orthogonal Multiple Access
OP	Outage Probability
PDF	Probability Density Function
PIN	Positive-intrinsic-negative
RIS	Reconfigurable Intelligent Surface
RV	Random variable
SINR	Signal-to-interference-noise-ratio
SNR	Signal-to-noise-ratio

List of Figures

Figure 1.1: RIS structure 11
Figure 1.2: A single passive element of RIS 12
Figure 1.3: User at dead zone 14
Figure 1.4: Physical layer security. 15
Figure 1.5: User at cell edge. 15
Figure 1.6: Massive device-to-device communications. 16
Figure 3.1: Distribution of Z RV for n $\in$ 1,2,3, m $=$ 2, and N = 4. 36
Figure 3.2: Outage probability analysis for different n parameter. 37
Figure 3.3: Outage probability for different m parameter. 38
Figure 3.4: Outage probability versus rate threshold. 39
Figure 3.5: Outage probability analysis for different N parameter. 40
Figure 3.6: Distribution of X RV 43
Figure 3.7: Distribution of Y RV 44
Figure 3.8: Received power for Bob positioned at 0°. 44
Figure 3.9: Received power for Bob positioned at 30° 45
Figure 3.10: Received power for Bob positioned at 45°. 45
Figure 3.11: Received power for Bob positioned at 60°. 46
Figure 3.12: Received power for Eve positioned at 0°. 46
Figure 3.13: Received power for Eve positioned at 30°. 47
Figure 3.14: Received power for Eve positioned at 45°. 47
Figure 3.15: Received power for Eve positioned at 60°. 48

List of Tables

Table 3.1: Obtained total errors for the results in Figures 3.2, 3.3, and 3.5……42

Table 3.2: Comparison of received powers for Bob and Eve……49

Table 3.3: Received power when RIS partitioning is used……..…..50

Chapter 1 – Introduction

1.1 Background

Wireless communication is the exchange of information between two or more points using electromagnetic waves, including radio frequencies, microwaves, and infrared frequencies. Examples of wireless communications technologies include radio frequency communication, cellular networks, Bluetooth, Wi-Fi, infrared communication, satellite communication, near-field communication, wireless local area networks, and microwave communication. A particular type of wireless communication is cellular networks, which provide communication services for mobile devices such as smartphones and tablets through voice calls, messaging, and internet connections. Cellular networks enable communication over large distances by dividing areas into smaller segments called cells, each connected to a base station (BS). BSs are interconnected to provide continuous communication over a wide geographical region. Cellular networks are an essential component of contemporary communication systems and have progressed through various generations. For example, first generation (1G) networks were analog and supported only voice calls, while second generation (2G) networks were digital and provided services such as text messaging and basic internet access. The third and fourth generations (3G and 4G) supported video calls, mobile internet, and provided significantly increased data rates and quality. The latest development, called fifth generation (5G), offers even faster data speeds, greater connectivity and low latency, ensuring high-quality performance for today's applications. 5G networks are made to work with cutting edge technologies like Internet of Things (IoT) , self-driving cars, and smart technologies [1]. The next evolutionary step in wireless communication is sixth generation (6G) that aims to further develop the capabilities of cellular networks. It is expected that 6G networks will offer very fast speeds, minimal latency, ubiquitous connectivity, enhanced security, and privacy [2].

The progression of 6G networks encompasses the incorporation of state-of-the-art technologies such as terahertz frequencies, advanced antenna designs, artificial intelligence, network slicing, and reconfigurable intelligent surface (RIS). These innovations collectively allow 6G to surpass the capabilities of 5G in terms of speed, connectivity, latency, and more. This thesis work investigates one of the key enablers of 6G, namely RIS, and provides detailed analysis for the performance of RIS-aided systems.

1.2 Fundamental Principles of RIS

RIS is developing as a crucial hardware enabler in the realm of 6G networks, with tremendous potential to improve wireless communication networks [3]. The surface is made up of several tiny passive parts that can influence and regulate electromagnetic radiation. These components can change the phase, amplitude, and polarization of incoming electromagnetic waves, allowing them to affect the direction of signal propagation. RIS provides the following advantages to 6G networks: greater coverage, energy efficiency, higher capacity and throughput, decreased interference, and support for huge connection. This surface may increase the coverage area of BS by intelligently reflecting signals to non-line-of-sight (NLoS) areas. This is particularly important in cities with complex infrastructure. In addition, as compared to the traditional methods of wireless communication, RIS can direct the signals more effeciently, thereby lowering the energy consumption of the networks and significantly increasing wireless network data rates and capacity. Moreover, RIS controls signal direction and characteristics to reduce interference and improve the quality of service for applications. Also, RIS can manage complex environments with high desnity of connected devices, such as IoT applications, and can provide reliable connections for all users. In general, RIS has many advantages to boost wireless communication to the next level.

1.2.1 Hardware Architecture of RIS

RIS is composed of three layers: the inner layer, the copper plate, and the outside layer as shown in Figure 1.1. These three layers together called “metasurface”, which is a network of metaatoms with electrical thickness on a subwavelength scale of the corresponding frequency that can be electronically controlled [4]. Metasurface poses requiring properties such as low loss at the operational frequencies and ease of integration with electronic components. The outer layer of the RIS contains many passive elements that can directly interact with the signals. On top of this layer there is a copper plate that blocks the energy of the signal. The last layer, the inner layer, comprises a control board that adjusts the phase shift and reflection amplitude of each element. The inner layer is connected to the controller to to individually control the state (e.g., reflection phase shift) of each metaatom. This allows for dynamic reconfiguration of the passive elements.

Figure 1.2 illustrates the shape of a single passive element. This element is fitted with a PIN diode that controls the reflection of incoming waves. The RIS controller may switch this PIN diode "on" and "off" depending on the BS and end-user's channel state information (CSI). This RIS controller can alter the bias voltages for each RIS element, facilitating the reconfiguration process [5]. However, adjusting the phase shift and reflection amplitude of each passive element of the RIS is costly but enhances transmission. For high-precision, the

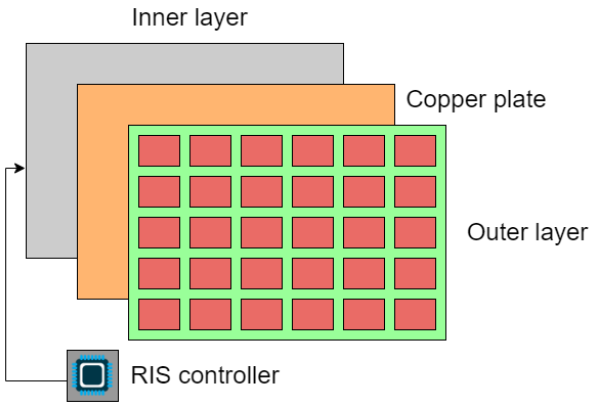

Figure 1.1: RIS structure

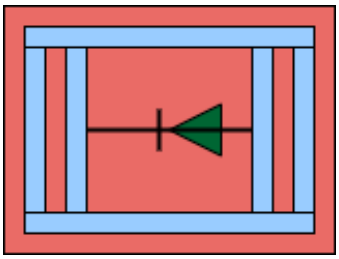

Figure 1.2: A single passive element of RIS

number of integrated PIN diodes shoud be increased and advanced computation methods need to be used as RIS controller requires more operating pins to enable a large number of PIN diodes [6]. For example, RIS element with five PIN diodes gives a total of 32 phase shifts, which provides better performance as compared to RIS element with one PIN diode and two phase shift variations.

1.2.2 Main challenges in designing and implementing RIS

RIS provides many advantages for wireless communication, but there are key issues involved in the design and implementation of RIS. These challenges include hardware design and fabrication, channel estimation and signal processing, and passive beamforming design.

There are many challenges in hardware design and fabriciation including material selection, design of passive elements, and manufacturing techniques. Material selection is important process because chosen materials should have right electromagnetic properties to allow dynamic control of phase, amplitude, and polarization of incoming electromagnetic waves. In addition, selected materials must resist environmental factors such as temperature variations and humidity while keeping the same performance. To design passive element that can well function over a broad range of frequencies and environmental conditions is a challenging task. These passive components should be tiny enough to interact with electromagnetic waves in the mmWave and terahertz frequency regions, where future wireless networks are predicted to function. The precise manufacture of these components, while

simultaneously ensuring that they are both cost-effective and long-lasting, adds a new element of complexity.

RIS can regulate and modify incoming electromagnetic waves utilizing deep knowledge of the wireless channel gained via modern channel estimation methods and signal processing algorithms. However, utilizing sophisticated techniques for channel estimate is difficult because to the high dimensionality, passive nature of RIS, dynamic wireless environment, hardware flaws, and ambient influences. The number of passive elements define dimentionality for the channel estimation problems, because each passive element parameters are calculated independently. The large number of passive parts creates a high-dimensional optimization issue for channel estimation, which is a computationally demanding operation. Furthermore, RIS is passive and has no signal processing capabilities, complicating the computation of channel status information between transmitter, RIS, and receiver. In addition, since wireless channels are dynamic, channel estimate must be conducted on a regular basis, which may increase computing complexity and overhead.

Beamforming is a method for transmitting or receiving signals in certain directions while reducing interference from other directions, resulting in improved signal quality and system performance. The design of passive beamforming for RIS faces challenges because to the distinct levels of amplitude and phase shift. In discrete sets, an effective approach includes working with continuous amplitude and phase-shift values, as well as rounding findings to the nearest integer. This reduces the time required to complete computations, but it may result in decreased performance owing to quantization mistakes. To optimize network performance, a RIS's passive reflect beamforming should be synced with the transmit beamforming of other active components, such as a BS. When the BS's direct connection to the user is limited, transmit beamforming should be aimed toward the RIS to optimize signal reflection. When the BS-user connection's signal attenuation is comparable to the BS-RIS-user link, transmit

beamforming should balance the user and RIS directions. To improve signal reflection, adjust the reflection amplitude appropriately [7].

1.2.3 Applications of RIS

This section describes four applications of RIS that are used for different purposes, namely to enhance coverage and physical layer security, to assist user at cell egde, and to support massive device-to-device communication.

Figure 1.3 illustrates the scenario for expanding the coverage of BS by using RIS. The system model consists of BS, RIS, and user at dead zone. It is vital to remember that the direct connection between BS and the user is now restricted due to environmental constraints. RIS is used to create a virtual line-of-sight (LoS) connection between the BS and the user by intelligently routing the signal received from the BS to the user. Expanding coverage region by using RIS is especially useful for mmWave communications, because electromagnetic waves are susceptible to interference from obstacles.

The second use of RIS is to improve the physical layer security of the system, as indicated in Figure 1.4. The system comprises of BS, RIS, two users, and an eavesdropper. It is vital to note that when the eavesdropper is in the same signal propagation direction as the legitimate user (User 2) and the distance between BS and eavesdropper is less than the distance between BS and legitimate user (User 1), the system experiences security concerns. Physical

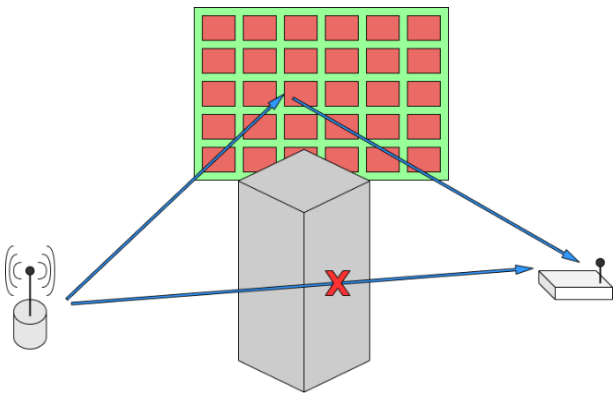

Figure 1.3: User at dead zone

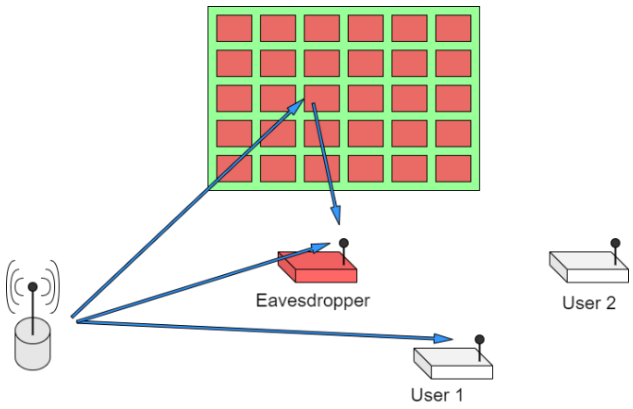

Figure 1.4: Physical layer security.

layer security may be strengthened by utilizing RIS since the signal reflected from RIS can be steered towards an eavesdropper, canceling out the valuable signal from the base station.

In the third application shown in Figure 1.5, the system model comprises of two BS, RIS, and two users. The cell-edge user (orange) encounters significant signal attenuation from its serving BS (blue), as well as interference from an adjacent BS (yellow). This problem may be resolved by deploying RIS near the cell-edge user (orange). RIS improves the signal received from the serving BS (blue) by routing the whole signal to the cell-edge user (orange). Furthermore, RIS reduces the signal received by the adjoining BS (yellow) and filters out interference.

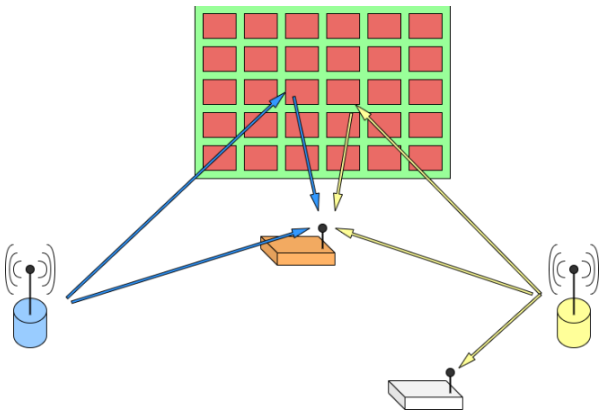

Figure 1.5: User at cell edge.

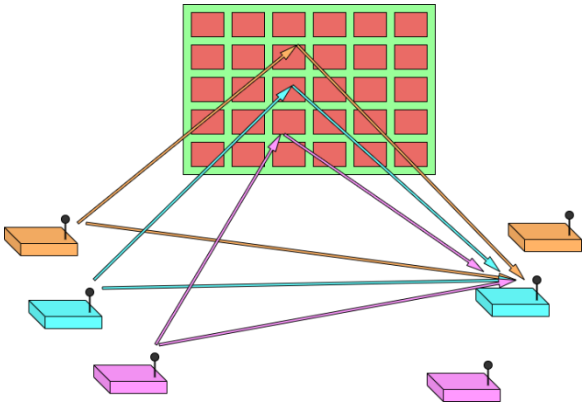

Figure 1.6: Massive device-to-device communications.

Lastly, Figure 1.6 shows how RIS can facilitate huge device-to-device communications by facilitating simultaneous low-power device-to-device transmissions via interference reduction and acting as a signal reflection hub.

1.3 Aims and Objectives

This project aims to study and assess the potential of RIS as a technology that may significantly improve the performance, efficiency, and capacities of future wireless networks. The first goal is to comprehend the integration of RIS into current and next wireless networks for enhancing signal quality, energy efficiency, and network coverage. Secondly, the aim is to measure the performance of RIS technology in terms of evaluation metrics of wireless communication, namely OP. Thirdly, the objective is to examine the technical and practical difficulties related to the implementation of RIS technology and provide feasible remedies. Lastly, to investigate the ways in which RIS might enhance the scalability, flexibility, and sustainability of future wireless networks.

In order to accomplish the aforementioned goals, the following objectives will be pursued. The first step is to conduct literature review for the existing research works, projects, and case studies on RIS in order to identify the present capabilities, limits, and areas that may be enhanced. Next, examine the fundamental basic concepts that form the basis of RIS technology, including as phase shifters and the manipulation of electromagnetic waves.

Thirdly, explore two important system models related to future wireless networks, namely cascaded RIS-aided system and RIS-partiotioning system. The next step is to mathematically evaluate these system models and provide performance analyzes by using OP metric. The final step is to assess and compare obtained closed-form expressions with the Monte-Carlo simulations.

1.4 Literature Review

RIS-aided systems have been investigated from many aspects, including path loss modeling, combined performance with MIMO technology, security, beamforming, and practical implementation. The literature review was conducted for three research areas of RIS, namely channel modeling, multi-RIS-aided system, and RIS partitioning.

The statistical analysis of random wireless channels and the performance assessment of RIS-aided networks have been extensively studied in [8]–[16]. In [8], RIS-aided multi-user multiple-input single-output (MISO) network with coupled Rayleigh fading distribution and poor CSI was studied. The authors developed a closed-form statistical formula for the possible spectral efficiency and demonstrated that output is dependent on training overhead and statistics. RIS and massive MIMO systems were researched for channel estimation and closed-form channel statistics were derived for the uplink (UL) and downlink (DL) ergodic capacity [9]. The authors figured out that RIS is beneficial when the access points-user links are insecure. In [10], closed-form OP was derived for the RIS-aided system with Rician fading distribution. Aside from that, analytical formulas were developed for the Rician fading parameters, which are dependent on phase-alignment precision and the number of elements. In [11], the benefits of various RIS-aided wireless networks, as well as the direct connectivity between transmitter and receiver, were investigated. The findings indicated that the RIS and direct link network had lower symbol error probabilities than the old system for the same transmission power. The authors in [12] presented RIS's working principles, metasurface and

reflectarray implementations, channel models, and correct channel estimations. It contrasts RIS optimization with standard MIMO array precoding, emphasizing obstacles and potential. Numerical findings show the RIS's influence on MIMO channel characteristics. In [13], the paper discussed open research questions, gives an outline of current solutions, and uses mathematical methods to look into the theoretical performance limits of multiple RIS-assisted communication systems. In [14], a comprehensive introduction to RIS-assisted wireless communication was provided, including topics such as hardware architecture, channel estimation, and reflection optimization. In [15], the letter shows correct closed-form estimates for channel distributions in two RISs-based wireless system configurations: RIS - dual-hop and RIS - transmit. Based on the performance study, the diversity orders that can be reached for the RIS - dual-hop and RIS - transmit schemes. Both approaches provide the same level of diversification increases. RIS - Dual-hop channels resemble keyhole MIMO channels with one degree of freedom. In [16], the study looked at two transmission scenarios including RIS, one in which RIS serves as a relay and the other as a transmitter source, and how these systems' channels are distributed.

Several papers [17]–[19] looked at the phase shifts caused by RIS's reflective parts, and they found that there were phase errors because there weren't enough available phase shifts. In [17], the research looks at how well a single-input single-output system works with a large intelligent surface that can be used as a controlled scatterer. It takes into account quantization phase errors and the fact that there are no direct links between the devices that are sending and receiving. The paper provides closed-form formulae for the average symbol error rate, OP, and spectral efficiency. Monte Carlo simulations reveal that the approach is quite precise and investigate the power scaling law and the amount of space required. According to the findings, a normal system without a big intelligent surface performs poorly compared to one with around fifty elements and four specific bits for phase quantization. In [18], the study looked at a RIS-

assisted single-input, single-output system across Rayleigh fading channels. This model examines the interaction of amplitude and phase response to produce closed-form formulae for OP and ergodic capacity. The study simplifies formulae for numerous reflecting components and provides tight upper and lower bounds on ergodic capacity. In [19], the performance of a RIS-assisted communication system over Rician fading channels is investigated utilizing statistical channel state information in this research. In the high SNR area, it produces an asymptotic outage probability expression as well as an approximate closed-form expression of outage probability. Channel gain grows exponentially and linearly with the number of reflecting components, but diversity gain has no influence on the number of reflecting elements. Although a single RIS-aided system with phase faults was investigated in [19], the channel was modeled using Rayleigh fading. The Nakagami-m fading distribution best represents the features of LoS communication seen in RIS-assisted networks.

While prior research has undoubtedly contributed significantly to the domain of RIS, its emphasis has been on system models featuring a single RIS. At present, only a limited number of works are contemplating the implementation of multi-RIS [20]-[22]. For example, the ergodic capacity and OP of a network consisting of numerous RISs linked in series between the transmitter and receiver were measured by the authors in [20]. Furthermore, for cascaded RIS-aided systems, the investigation of passive beamforming and beam routing was conducted with the highes SNR in [21] and [22].

RIS partitioning system with NOMA users have been extensively investigated in [23]-[27]. RIS partiotining is used to simultaneoudly serve NOMA users while keeping the quality-of-service os wireless communication. In [23], RISs are being researched to improve bidirectional NOMA networks. Partitioning RIS enhances channel conditions for NOMA users by increasing NOMA gain and eliminating UL power control. Under four operational regimes, optimal RIS partitioning and BS power regulation meet the UL-QoS and DL-QoS

requirements, respectively. In [24], RIS-aided NOMA downlink transmission system is presented. The system optimizes user segmentation and RIS phase shifting to enhance mobile user cumulative data rate in NOMA downlink networks. RIS phase shifting matrix optimization is presented using a deep deterministic policy gradient technique. In [25], article suggests a new NOMA approach for next-generation wireless communications that uses RIS splitting that can be changed. The system gives real resources to different users. For example, the base station and RIS are each allocated to a separate cluster. It is feasible to create an optimization problem that optimizes user fairness by allocating RIS portions to various users. The system is explored utilizing effective search algorithms, and simulations reveal improved performance in terms of ergodic sum-rate, OP, and user fairness. In [26], the study looked at a grant-free non-orthogonal multiple access (GF-NOMA) approach that employs a customisable RIS. To get the maximum network sum rate, it recommends combining user grouping with RIS assignment or alignment. This technique matches user devices with varied channel gains, assigns RISs to the appropriate groups, and aligns RIS phase changes with cluster members. Depending on the network specifics, this strategy may result in a 20% higher network sum rate than regular GF-NOMA and grant-based optimum PD-NOMA methods. In [27], the paper investigates how RIS technology might improve wireless communication. Using electromagnetic signal manipulation, RISs may control the wireless channel and give benefits. Active RIS designs eliminate double fading and other issues. A hybrid RIS system with power differential over-the-air achieves simulated NOMA. The RIS's active and passive features allow users with equal transmit power, route loss, and distance to connect to a base station while sharing time and frequency resources. The two-user system model is shown.

In wireless communication, channel state information (CSI) represents the combined effects of scattering, fading, and power degradation. RIS is passive by nature, thus the system needs efficient algorithms to calculate CSI. Perfect CSI knowledge is important for evaluating

the system performance, especially it is important to design beamforming [28]–[31]. In [28], the RIS-aided large MIMO system used deep reinforcement learning to calculate the transmit beamforming and phase-shift matrix. The scientists discovered that optimal neural network settings considerably improve the model's performance and produce equivalent results to state-of-the-art models. In [29], a DL model was designed to form beamforming in RIS-aided networks. The constructed model was trained using unsupervised learning, but it can make immediate decisions when trained online. The output showed that the developed model reduces computational complexity when compared with the traditional semi-definite relaxation approach. In [30], a DL model was developed for active/passive beamforming of RIS-aided multi-user MISO system. Simulation results showed that the developed model is less computationally complex as compared to iterative optimization algorithms. In [31], compressive sensing and DL models were developed to construct the channels and then to operate with the incoming rays in large intelligent surface aided systems. As simulation results reveal the developed models can achieve faster data rates.

The research will enhance the existing knowledge on RIS and its capacity to transform wireless communications, hence facilitating the development of more effective, adaptable, and environmentally friendly networks. This thesis work investigates cascaded RIS-aided system by considering phase errors generated from the limitations of RIS. Also, the paper provides analytical and experimantal analysis for RIS partitioning system that cosidereds imperfect CSI because of the mobility of the users.

The organization of this thesis work is following: In chapter 2, the methodology of the research is explained for cascaded RIS-aided system and RIS partitioning system. In chapter 3, obtained results are illustrated and discussed in detail for both system models. The thesis conclusion is provided in chapter 4.

Chapter 2 – Methodology

This chapter describes two system models, namely cascaded RIS-aided system, and RIS partitioning system, and provides methods to evaluate and analyze these models. Both models are important to investigate in order to obtain useful insights. Cascaded RIS-aided system has been investigated by conisdering phase-errors generated because of the quantization errors. For the RIS partitioning system both experimental and analytical analysis are performed. In addition, analytical derivations were validated by Monte-Carlo simulations.

2.1 Cascaded RISs-aided system

A cascaded RIS-aided system is a network of RISs connected in sequence. Figure 2.1 depicts the system model, which includes BS, n RISs (each RIS has N reflecting components), and a user. It is vital to note that the direct connection between BS and the user is hindered due to environmental constraints. The user position is only accessible to the final RIS in the series. The channels from other RISs to the user are unavailable. This system type is used to increase the coverage of BS and is particularly beneficial in densely populated regions. The performance of this system architecture is evaluated using the outage probability measure. To determine the likelihood of an outage, the PDF of the end-to-end channel from BS to user was calculated. The random channels between BS and RIS-1 are expressed as

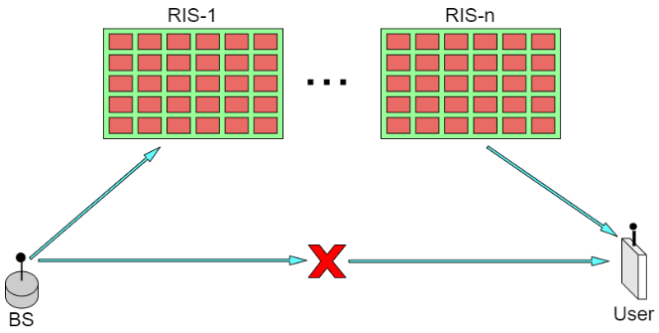

Figure 2.1: A cascaded RIS-aided wireless network.

$$h = |h_i|e^{j\phi_i}, \tag{2.1}$$

where h is set of N complex random variables (RVs) and $i \in \{1, 2, 3, \dots, N\}$. The channel entities between two adjacent RISs (e.g. RIS-i and RIS-(i+1)) is represented by

$$G_j = |g_{il}|e^{j\theta_{il}}, \tag{2.2}$$

where G_j is complex $N \times N$ RVs, $i, l \in \{1, 2, 3, \dots, N\}$, and $j \in \{1, 2, 3, \dots, n-1\}$. Finally, the random channel between the last RIS in the row and end-user is represented by

$$q = |q_k|e^{j\psi_k}, \tag{2.3}$$

where q is set N of complex RVs and $k \in \{1, 2, 3, \dots, N\}$. It is assumed that RISs have the same number of reflecting passive elements ($N = N_1 = N_2 = \cdots = N_n$). The distances that correspond to these are represented by $d_{BS\to RIS-1}$, $d_{RIS-1\to RIS-2}$, …, $d_{RIS-n\to user}$. It is believed that all connections have the same path-loss coefficient, denoted as τ. All the channels stated above are modeled by independent and identically distributed Nakagami-m distribution. The probability density function (PDF) of Nakagami-m RV is defined as

$$f_X(x) = \frac{2m^m}{\Gamma(m)\Omega^m} x^{2m-1} e^{-\frac{m}{\Omega}x^2}, \tag{2.4}$$

where X is positive RV, $\Gamma(\cdot)$ is the Gamma function [32, (8.310)]; $m \geq 1/2$ and $\Omega > 0$ are the corresponding shape and spread parameters. The moments of Nakagami-m RV can be defined as

$$\mathbb{E}[X^p] = \left(\frac{\Omega}{m}\right)^{\frac{p}{2}} \frac{\Gamma\left(m + \frac{p}{2}\right)}{\Gamma(m)}, \tag{2.5}$$

where p is the moment order. The received signal by user can be mathematically expressed as

$$y = \sum_{i=1}^{N}\sum_{l=1}^{N} \dots \sum_{k=1}^{N} \overline{P}\, X_{il\dots k} e^{j\delta_{il\dots k}} \chi + n_{user}, \tag{2.6}$$

where χ, and n_{user} are stand for transmitted symbol and AWGN of end-user with zero mean and variance of σ_{user}^2, respectively. $X_{il\dots k} = |h_i|\left|g_{il}^{G_1}\right| \dots |q_k|$ and $\delta_{il\dots k} = \phi_i - {\alpha_i}^{R_1} + {\theta_{il}}^{G_1} + \cdots - {\alpha_k}^{R_n} + \psi_k$ is the phase error. Also, $\overline{P}$ stands for the normalized transmit power and defined as

$$\overline{P} = \sqrt{\frac{P}{d_{BS\to RIS-1}^{\tau} d_{RIS-1\to RIS-2}^{\tau} \cdots d_{RIS-n\to user}^{\tau}}}, \tag{2.7}$$

where *P* is the transmit power.

For cascaded RIS-aided system model, the phase errors are unavoidable for the following two reasons. First, elements of RIS can adjust the phase of only one path at a certain time, but in cascaded RIS-aided system N^n paths are established simultaneously. There are only $n \times N$ number of phases that can be adjusted by the elements of RIS and the remaining $N^n - n \times N$ paths certainly have phase errors. The second reason is RIS elements can not adjust any phase because it is limited to the discrete set. For instance, 2-bit RIS element can only adjust four phases. In general, number of available phases, *Q*, and number of bits, *b*, relate to each other by $Q = 2^b$. Therefore, phase errors always present in cascaded RIS-aided systems. These phase errors are modeled with the uniform distribution. Its PDF is given by

$$f_{\delta_{il\dots k}}(\delta) = \frac{Q}{2\pi}, -\frac{\pi}{Q} \le \delta \le \frac{\pi}{Q}, \tag{2.8}$$

The SNR at end-user can be given by

$$\gamma = \frac{\overline{P}\left|\sum_{i=1}^{N}\sum_{l=1}^{N}\cdots\sum_{k=1}^{N} X_{il\dots k} e^{j\delta_{il\dots k}}\right|^2}{\sigma_{user}^2}, \tag{2.9}$$

To evaluate and analyze the system performance, the OP metric is used. The OP is defined as

$$P_{\text{out}}(\gamma_{th}) = \Pr[\gamma < \gamma_{\text{th}}]$$
$$= \Pr\left[\frac{\overline{P}Z^2}{\sigma_{user}^2} < \gamma_{\text{th}}\right]$$
$$= \Pr\left[Z < \sqrt{\frac{\gamma_{\text{th}}\sigma_{\text{user}}^2}{\overline{P}}}\right]$$
$$= \int_0^T f_Z(z)dz, \tag{2.10}$$

where $Z = \left|\sum_{i=1}^{N}\sum_{l=1}^{N}\dots\sum_{k=1}^{N} X_{il\dots k}e^{j\delta_{il\dots k}}\right|$, $T = \sqrt{\frac{\gamma_{\text{th}}\sigma_{\text{user}}^2}{\overline{P}}}$, $f_Z(z)$ is PDF of Z, and $\gamma_{\text{th}} = 2^{R_{\text{th}}} - 1$, where R_{th} is the desired rate threshold. It is difficult, if not impossible, to find closed-loop PDF of Z, thus we find approximate PDF of Z. Using MATLAB's distribution fitting tool, it was shown that the PDF of Z may be well represented by the Gamma distribution, which is defined as

$$f_Z(z) = \frac{z^{\alpha-1}\beta^{\alpha}}{\Gamma(\alpha)}e^{-\beta z}, \tag{2.11}$$

where $\alpha > 0$ and $\beta > 0$ are corresponding shape and scale parameters. From (2.10) and (2.11), the closed-form OP is defined as

$$P_{\text{out}}(T) = \frac{\gamma(\alpha, \beta T)}{\Gamma(\alpha)}, \tag{2.12}$$

where $\gamma(.,.)$ is the lower incomplete Gamma function [32, (8.350.1)]. By using moment matching method (MMM), α and β parameters are defined as

$$\alpha = \frac{-\mathrm{E}[Z^4] + 5\mathrm{E}[Z^2]^2 + U}{2\mathrm{E}[Z^4] - 2\mathrm{E}[Z^2]^2}, \tag{2.13}$$

$$\beta = \sqrt{\frac{2\mathrm{E}[Z^4] + 2\mathrm{E}[Z^2]^2 - U}{6\mathrm{E}[Z^2]}}, \tag{2.14}$$

where $U = \sqrt{\mathrm{E}[Z^4]^2 + 14\mathrm{E}[Z^4]\mathrm{E}[Z^2]^2 + \mathrm{E}[Z^2]^4}$. To find α and β parameters, first we need to find the second and the fourth moments of Z RV, which are calculated as

$$\mathrm{E}[Z^2] = N^n \left(\frac{\Omega}{m}\right)^{n+1} \left(\frac{\left(\Gamma(m+1)\right)^{n+1}}{\left(\Gamma(m)\right)^{n+1}} + (N^n - 1) \frac{\left(\Gamma\left(m+\frac{1}{2}\right)\right)^{2n+2}}{\left(\Gamma(m)\right)^{2n+2}} \frac{Q^2 \sin^2\left(\frac{\pi}{Q}\right)}{\pi^2} \right), \quad (2.15)$$

$$\mathbb{E}[Z^4] = (N^n - 1)N^n \left(\frac{\Omega}{m}\right)^{2n+2} \left(\frac{\left(\Gamma(m+2)\right)^{n+1}}{\left(\Gamma(m)\right)^{n+1}(N^n - 1)} + \frac{\left(\Gamma(m+1)\right)^{2n+2}}{\left(\Gamma(m)\right)^{2n+2}} \right.$$

$$+4 \frac{\left(\Gamma\left(m+\frac{3}{2}\right)\right)^{n+1}}{\left(\Gamma(m)\right)^{n+1}} \frac{\left(\Gamma\left(m+\frac{1}{2}\right)\right)^{n+1}}{\left(\Gamma(m)\right)^{n+1}} + 2(N^n - 2) \frac{\left(\Gamma(m+1)\right)^{n+1}}{\left(\Gamma(m)\right)^{n+1}} \frac{\left(\Gamma\left(m+\frac{1}{2}\right)\right)^{2n+2}}{\left(\Gamma(m)\right)^{2n+2}}$$

$$\times \frac{Q^2 \sin^2\left(\frac{\pi}{Q}\right)}{\pi^2} + 2 \frac{\left(\Gamma(m+1)\right)^{2n+2}}{\left(\Gamma(m)\right)^{2n+2}} \frac{8\pi^2 + Q^2 - Q^2 \cos\left(\frac{4\pi}{Q}\right)}{16\pi^2} + 4(N^n - 2) \frac{\left(\Gamma(m+1)\right)^{n+1}}{\left(\Gamma(m)\right)^{n+1}}$$

$$\times \frac{\left(\Gamma\left(m+\frac{1}{2}\right)\right)^{2n+2}}{\left(\Gamma(m)\right)^{2n+2}} \frac{Q^2 \sin^2\left(\frac{\pi}{Q}\right)\left(2\pi + Q \sin\left(\frac{2\pi}{Q}\right)\right)}{4\pi^3} + (N^n - 2)(N^n - 3)$$

$$\left. \times \frac{\left(\Gamma\left(m+\frac{1}{2}\right)\right)^{4n+4}}{\left(\Gamma(m)\right)^{4n+4}} \frac{Q^4 \sin^4\left(\frac{\pi}{Q}\right)}{\pi^4} \right). \quad (2.16)$$

The approximation by using MMM is only valid for the sum of uncorrelated RVs. However, the generated $Z_{il\ldots k} = X_{il\ldots k} e^{j\delta_{il\ldots k}}$ terms are correlated between each other. Therefore, from obrained α and β parameters, we need to find α^* and β^* parameters that well approximates the sum of correlated RVs. To find these parameters, the mean and variance of Gamma distribution are used. The sum of correlated n*Nakagami-m RVs relate to the sum of uncorrelated RVs with following two expression. The first expression is defined as

$$\mathbb{E}[Z] = \alpha\beta = \alpha^*\beta^*. \tag{2.17}$$

The second one is dependence of variance of the sum of correlated and uncorrelated RVs, which is defined as

$$\text{var}\left(\sum_{i=1}^{N^n} Z_{i,\text{corr}}\right) = \text{var}\left(\sum_{i=1}^{N^n} Z_{i,\text{uncorr}}\right) + \sum_{i=1}^{N^n}\sum_{j=1,i\neq j}^{N^n} \text{cov}(Z_i, Z_j), \tag{2.18}$$

where $\text{cov}(Z_i, Z_j) = \mathbb{E}[Z_i Z_j] - \mathbb{E}[Z_i]\mathbb{E}[Z_j]$ is the covariance between two RVs. If we rewrite (2.18) in terms of α and β parameters then following relationship would be obtained

$$\alpha^*\beta^{*2} = \alpha\beta^2 + \sum_{i=1}^{n-1} N^n \frac{(i+1)}{(N-1)^{i-n}} \sin^2\left(\frac{\pi}{Q}\right)\left(\frac{\Omega}{m}\right)^{n+1}\left(\frac{Q}{\pi}\right)^2 \frac{\left(\Gamma\left(m+\frac{1}{2}\right)\right)^{2(n+i-1)}}{\left(\Gamma(m)\right)^{2(n+i-1)}}$$

$$\times\left[\frac{\left(\Gamma(m+1)\right)^i}{\left(\Gamma(m)\right)^i} - \frac{\left(\Gamma\left(m+\frac{1}{2}\right)\right)^{2i}}{\left(\Gamma(m)\right)^{2i}}\right]. \tag{2.19}$$

From (2.17) and (2.19), α^* and β^* parameters can be found accordingly

$$\alpha^* = \frac{\alpha\beta}{\beta^*}, \tag{2.20}$$

$$\beta^* = \beta + \frac{1}{\alpha\beta}\sum_{i=1}^{n-1} N^n \frac{(i+1)}{(N-1)^{i-n}} \sin^2\left(\frac{\pi}{Q}\right)\left(\frac{\Omega}{m}\right)^{n+1}\left(\frac{Q}{\pi}\right)^2 \frac{\left(\Gamma\left(m+\frac{1}{2}\right)\right)^{2(n+i-1)}}{\left(\Gamma(m)\right)^{2(n+i-1)}}$$

$$\times\left[\frac{\left(\Gamma(m+1)\right)^i}{\left(\Gamma(m)\right)^i} - \frac{\left(\Gamma\left(m+\frac{1}{2}\right)\right)^{2i}}{\left(\Gamma(m)\right)^{2i}}\right]. \tag{2.21}$$

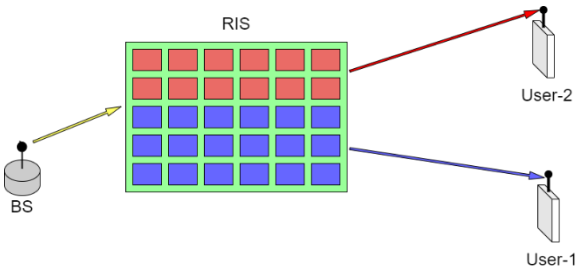

Figure 2.2: RIS partitioning system

These expressions would be used to find approximate Gamma distribution of the random channel generated from cascaded RIS-aided system.

2.3 RIS Partitioning System

RIS partitioning is the division of passive parts into separate portions, with each area dedicated to serving a specific user. The appealing attributes of RIS make it a very efficient remedy for the challenges faced by forthcoming wireless networks.

Figure 2.2 depicts a RIS partitioning system that comprises of the BS, RIS, and two non-orthogonal multiple access (NOMA) users (User-1 and User-2). It is considered that environmental constraints prevent the direct connection between BS and users. The only way that communication establishes is through RIS. RIS is divided into two sections to serve both users simultaneously. There are K_1 elements to serve User-1 (blue) and K_2 elements to serve User-2 (red).

The performance of RIS partiotioning system is evaluated by analytical and experimental approach.

2.3.1 Analytical Approach

Analytical analyzes are performed for the system model depicted in Figure 2.2. The channel between BS and RIS is denoted as h_k, and the channels between RIS and User-i is denoted by $g_{i,k}$. The received signal by each user can be mathematically derived as

$$y_i = \left[\sum_{k=1}^{K_1} g_{i,k} h_k \phi_i \, e^{j\theta_{i,k}} + \sum_{k=1+K_1}^{K} g_{i,k} h_k \phi_i \, e^{j\theta_{r,k}}\right] \times \sqrt{P_b}\left[\sqrt{\beta_1} x_1 + \sqrt{\beta_2} x_2\right] + n_i, \quad (2.22)$$

where K is the total number of RIS elements; $i, r \in \{1,2\}, i \neq r$; P_b is the transmitted power at BS; $\phi_i = d_{\text{BS}\to\text{RIS}}^{-\tau/2} d_{\text{RIS}\to\text{User}-i}^{-\tau/2}$, where $d_{\text{BS}\to\text{RIS}}$ and $d_{\text{RIS}\to\text{User}-\text{i}}$ are BS → RIS and RIS → User-i distances, accordingly; τ is the path-loss coefficients; $\theta_{i,k} = -\left(\arg\left[g_{i,k}\right] + \arg[h_k]\right)$; β_1 and β_2 are the BS power allocation coefficients, $\beta_1 + \beta_2 \geq 1$; x_1 and x_2 are corresponding messages of users; n_i is AWGN with zero mean and variance of σ_i^2. The signal to interference and noise ratio (SINR) for (2.21) is expressed as

$$\gamma_i = \frac{\beta_i P_b \left|\sum_{k=1}^{K_1} g_{i,k} h_k \phi_i \, e^{j\theta_{i,k}} + \sum_{k=1+K_1}^{K} g_{i,k} h_k \phi_i \, e^{j\theta_{r,k}}\right|^2}{\xi \beta_r P_b \left|\sum_{k=1}^{K_1} g_{i,k} h_k \phi_i \, e^{j\theta_{i,k}} + \sum_{k=1+K_1}^{K} g_{i,k} h_k \phi_i \, e^{j\theta_{r,k}}\right|^2 + \sigma_i^2}, \quad (2.23)$$

where the variable ξ determines the sequence in which the user cancels or encounters interference. Usually, the position of BS and RIS are fixed but users are mobile, thus imperfect CSI is considered for this system model. Imperfect CSI for $g_{i,k}$ can be modeled as

$$g_{i,k} = \rho_i \hat{g}_{i,k} + \sqrt{1 - \rho_i^2} \Delta g_{i,k}, \quad (2.24)$$

where ρ_i is correlation between $g_{i,k}$ and $\hat{g}_{i,k}$ and $\Delta g_{i,k}$ is CSI estimation error modeled as AWGN. The updated SINR for two users can be expressed as

$$\gamma_i = \frac{P_b \beta_i |X_i|^2}{P_b \beta_i |Y_i|^2 + \xi_i P_b \beta_r |X_i + Y_i|^2 + \sigma_i^2}, \quad (2.25)$$

where X_i and Y_i are

$$X_i = \left[\sum_{k=1}^{K_1} \rho_i \hat{g}_{i,k} h_k \psi_i e^{j\theta_{i,k}} + \sum_{k=K_1+1}^{K} \rho_i \hat{g}_{i,k} h_k \psi_i e^{j\theta_{r,k}}\right], \quad (2.26)$$

$$Y_i = \sqrt{1-\rho_i^2}\left[\sum_{k=1}^{K_1} \Delta g_{i,k} h_k \psi_i e^{j\theta_{i,k}} + \sum_{k=K_1+1}^{K} \Delta g_{i,k} h_k \psi_i e^{j\theta_{r,k}}\right]. \quad (2.27)$$

By using MATLAB's distribution fitting tool, it was found that the distribution of X_i RV can be well approximated by Gaussian distribution. The parameters of Gaussian distribution are defined as

$$\mu = \sqrt[4]{\frac{3}{2}\mathrm{E}[X^2]^2 - \frac{1}{2}\mathrm{E}[X^4]} \quad (2.28)$$

$$\sigma^2 = \mathrm{E}[X^2] - \sqrt{\frac{3}{2}\mathrm{E}[X^2]^2 - \frac{1}{2}\mathrm{E}[X^4]} \quad (2.29)$$

The second and fourth moments of X_i is expressed as

$$\mathrm{E}[|X_i|^2] = K\mathrm{E}[x_i^2] + K_1(K_1-1)\mathrm{E}[x_i]^2, x_i = \rho_i\left|\hat{g}_{i,k}\right||h_k|\psi_i \quad (2.30)$$

$$\mathrm{E}[|X_i|^4] = \left(K_1 + \frac{3}{8}K_2\right)\mathrm{E}[x_i^4] + 4K_1(K_1-1)\mathrm{E}[x_i^3]\mathrm{E}[x_i] + 3(3K_1(K_1-1) + 3K_1K_2 + \frac{3}{4}K_2(K_2-1)\Big)\mathrm{E}[x_i^2]^2 + \big(6K_1(K_1-1)(K_1-2) + 3K_1(K_1-1)\big)\mathrm{E}[x_i^2]\mathrm{E}[x_i]^2 + K_1(K_1-1)(K_1-2)(K_1-3)\mathrm{E}[x_i]^4 \quad (2.31)$$

The distribution of Y_i RV is well approximated by Gamma distribution. Gamma parameters are defined as

$$\alpha_Y = \frac{\mathrm{E}[Y^2]^2}{\mathrm{E}[Y^4] - \mathrm{E}[Y^2]^2} \quad (2.32)$$

$$\beta_Y = \frac{\mathrm{E}[Y^4] - \mathrm{E}[Y^2]^2}{\mathrm{E}[Y^2]} \quad (2.33)$$

The second and fourth moments of Y_i is expressed as

$$E[Y^2] = KE[y_i^2],\ y_i = \sqrt{1-\rho_i^2}|h_k|\psi_i \quad (2.34)$$

$$E[Y^4] = KE[y_i^4] + [2K_1(K_1-1) + 4K_1K_2 + 2K_2(K_2-1)]E[y_i^2]^2 \quad (2.35)$$

2.3.2 Experimental Approach

Experiment on the performance of RIS partitioning was conducted for the system model shown in Figure 2.3 for near-field and far-field communications. There were two users (Bob and Eve) situated in two different postions. Each user has its own codebook. The experiment setup consisted from the following items:

- Signal Generator Keysight VXG M9384B
- Signal Analyzer Keysight UXA N9040B
- Power Source (to power the RIS)
- 1-bit RIS with 400 elements
- Antennas Pasternack PE9851B/2F-20
- Cable with -3 dBm loss

Signal Generator parameters: Frequency: 27.5 GHz; Amplitude: 0 dBm; No modulation.

Signal Analyzer parameters: Frequency center: 27.5 GHz; Frequency span: 10 KHz; Resolution Bandwidth: 10 Hz.

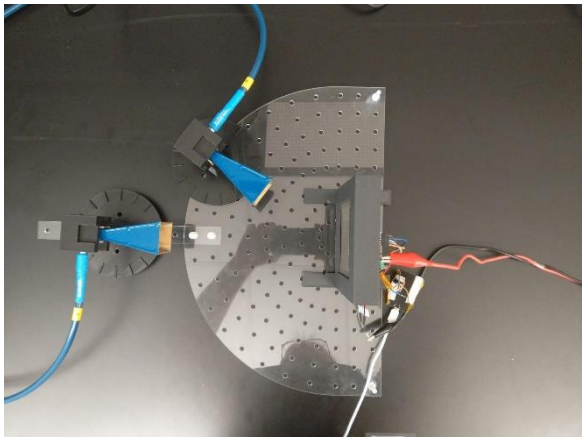

Figure 2.3: Transmitted at -30° and receiver (Bob) at 0°.

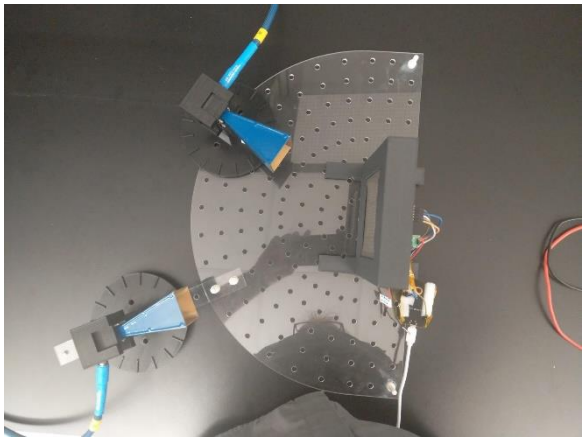

Figure 2.4: Transmitted at -30° and receiver (Eve) at 30°.

The experiment was performed by using above mentioned setups. Figure 2.3 and 2.4 illustrates the image of the constructed system model. Transmitted was constantly be located at -30°. The position of the receiver changed to four positions, namely 0°, 30°, 45°, and 60°.

Figure 2.5 illustrates the details of transmitter positioning. The Pasternack antenna was positioned at -30° and fixed. These antenna was connected to signal generator to transmit continuous sinusoidal signal at 27.5 GHz. The distance between transmitted and RIS is closer as compared to the distance between RIS and receiver.

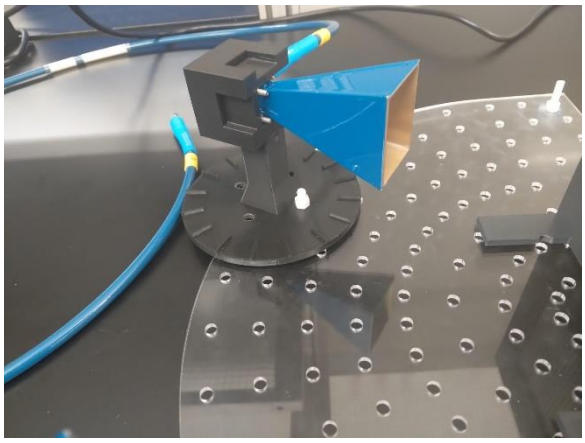

Figure 2.5: Details of transmitter positioning

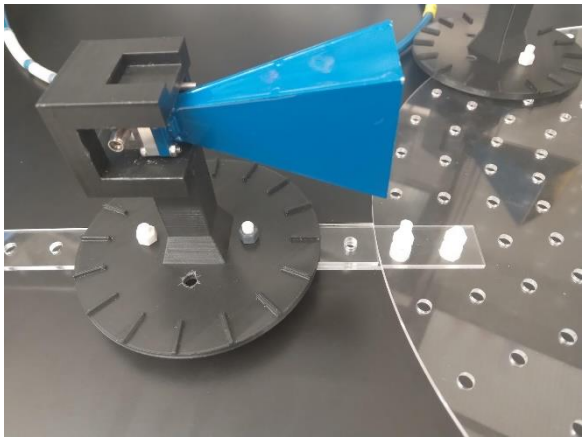

Figure 2.6: Details of receiver positioning

Figure 2.6 shows the details of the receiver positioning. The receiver is located at different angles and received power was recorded, respectively. The receiver antenna was connected to the signal analyzer to find the maximum signal at 27.5 GHz frequency.

Near–field communication: It is a short range wireless communication. Figure 2.7 shows the picture from the experiment. The distance to differentiate between near-field and far-field communications is calculated by using the following expression.

$$d = \frac{2D^2}{\lambda}$$
$$= \frac{2D^2 f}{c}$$
$$= \frac{2 * 0.047^2 * 27.5 * 10^9}{3 * 10^8}$$
$$= 1.21 \text{ m} \quad (2.36)$$

For near-field communication the distance should be less than 1.21 m. The transmitter antenna is positioned at -30° and 15 cm apart from the center of RIS. The transmitted signal is reflected by the RIS by using 200 codebooks, where each codebook is combination of on and off states. The receiver antenna is positioned 20 cm apart from the RIS and the received power is recorded at 0, 30°, 45°, and 60° angles from the RIS.

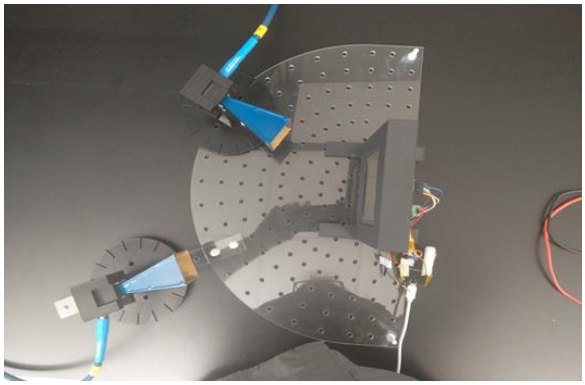

Figure 2.7: Near-field communication for RIS partitioning system

Far-field communication: It is a long-range wireless communication. Based on the characteristics of the antenna and the signal frequency, the far-field distance should be at least 1.2 m. In this experiment, the distance between transmitter and RIS is 2.2 m and the distance between RIS and receiver is 2 m to be in the safe side.

Figure 2.8 illustrates far-field RIS-aided communication experiment. For far-field communication only one case was checked where transmitter is located at -30° and the receiver is at 0° from the RIS. In this part, far-field distance was validated by transmitting different powers from the signal generator. In addition, the effect of RIS partitioning was analyzed for different combination of partitioning.

Figure 2.8: Far-field communication for RIS partitioning system.

Chapter 3 – Results & Discussions

This chapter presents the results and analysis for the two system models discussed in the methodology section.

3.1 Cascaded RISs-aided system

This part shows some modeling and analysis results for the cascaded RIS-aided system. The system was analysed up to n RISs, $n \in \{1, 2, 3\}$, where each located $d_i = 50$ m, $\forall i \in \{1, 2, \dots, n, n+1\}$ apart from each other. The channels are modeled by Nakagami-m RVs with following parameters $m \in \{2, 3, 4, 5, 6\}$ and $\Omega \in \{1, 2, 3, 4, 5, 6\}$, where m is responsible for number of paths between BS and user, and Ω is avearge received power. Number of passive elements per RIS is N, where $N \in \{4, 8, 16, 32, 64\}$ and reflecting coefficient for all elements are equal, $\eta = 1$. The path loss is equal for all channels, $\tau = 3$, and the desired rate threshold is $R_{\text{th}} = 3$ bits/s/Hz. The noise at the user side is $\sigma^2_{noise} = -70$ dBm, and it is assumed that 2-bit RIS elements are used with Q = 4 available options for phases.

Figure 3.1 illustrates the distribution of Z RV (curve) and its corresponding approximation found analytically (circle) when $n \in \{1,2,3\}, m = 2$, and N = 4. When n = 1, the distribution of Z RV ranges from 0 to 8. The peak of the distribution is obtained when z = 3 and its corresponding probability is 0.46. For the system model, when two RISs were used, the distribution of Z RV ranged from 0 to 32 with peak value obtained at z = 12 and correponsing probability is 0.12. The last case when n = 3, the maximum probability of 0.03 is obtained at z = 45, where $0 \leq z \leq 120$. For all three plots as number of RISs increase, the range of Z RV spreads. Analytical distribution shown by circles well matches with the simulational results. The approximation accuracy was validated by Kolmogorov-Smirnov (KS) goodness-of-fit-test.

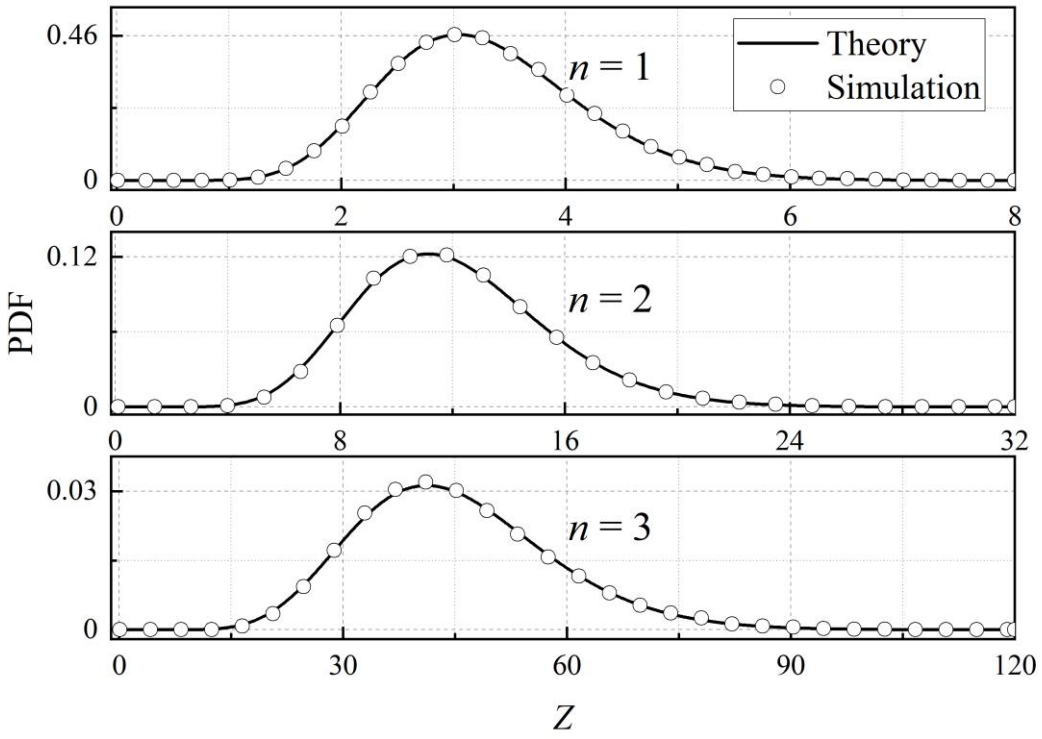

Figure 3.1: Distribution of Z RV for $\boldsymbol{n \in \{1,2,3\}, m = 2}$, and N = 4.

3.1.1 KS goodness-of-fit test

The KS goodness-of-fit test is used to check the accuracy of the approximation. The test compares critical value $D_{\max}$ and D, which are calculated as

$$D_{\max} \approx \sqrt{-\frac{\ln\left(\frac{\alpha}{2}\right)}{2L}} \tag{3.1}$$

$$D \triangleq \max|F_Z(z) - F_{\hat{Z}}(z)| \tag{3.2}$$

where L and α are sample size and confidence interval, respectively [33]; $F_Z(z)$ and $F_{\hat{Z}}(z)$ are corresponding exact and approximated CDFs of Z RV. The approximation is valid when the $D_{\max}$ > D. Let's examine the system that consists of two RISs and a total of four reflecting components for each RIS. The KS test statistic, D, for this system model is equal to 0.8×10^{-3}.

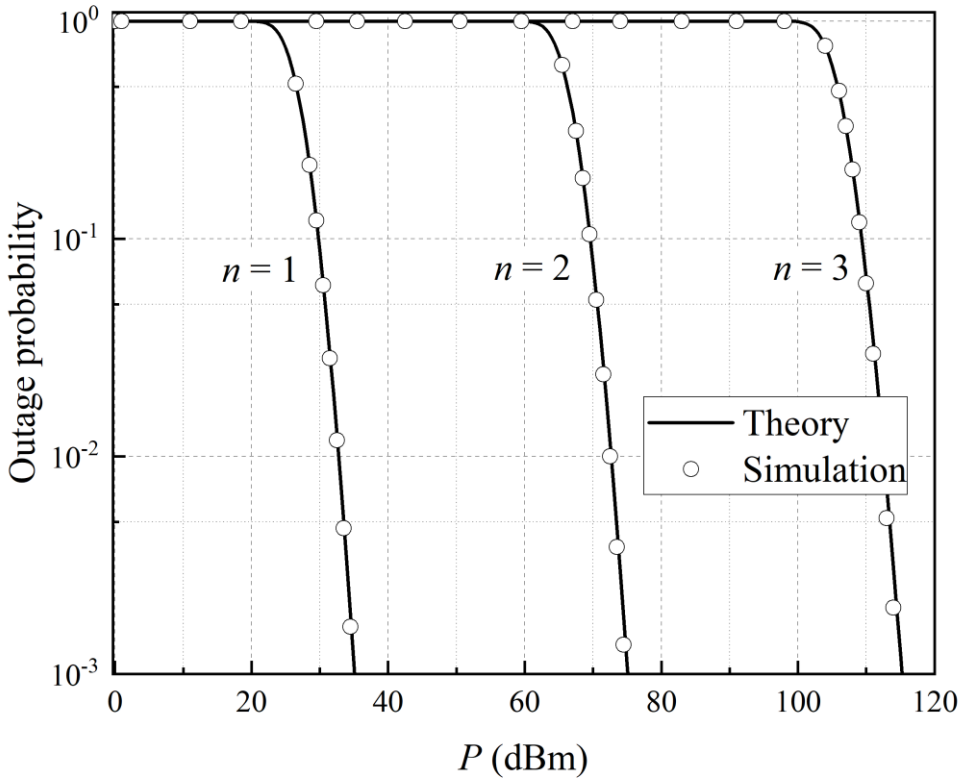

Figure 3.2: Outage probability analysis for different n parameter.

In the simulation, we set $L = 10^6$ and $\alpha = 0.05$. Using (3.1), $D_{\max} = 1.4 \times 10^{-3}$, which is greater than D, therefore the approximation is valid.

3.1.2 Performance analysis

The performance of the system model is evaluated in terms of OP metric. In this section, the influence of the parameters of the system are examined.

Figure 3.2 illustrates the perfromance analysis of cascaded RISs-aided system by varying number of RISs between BS and user. Three plots are depicted for the corresponding three system models when $n \in \{1, 2, 3\}$. In addition, for each case RIS with four reflecting elements are examined. The Nakagami-m shape and spread parameters are $m = 2$ and $\Omega = 1$. The system model with single RIS achieves OP of 10^{-3} at 35 dBm transmitted power. The same OP is achieved at 75 dBm for the cascaded RISs-aided system with two RISs. When n =

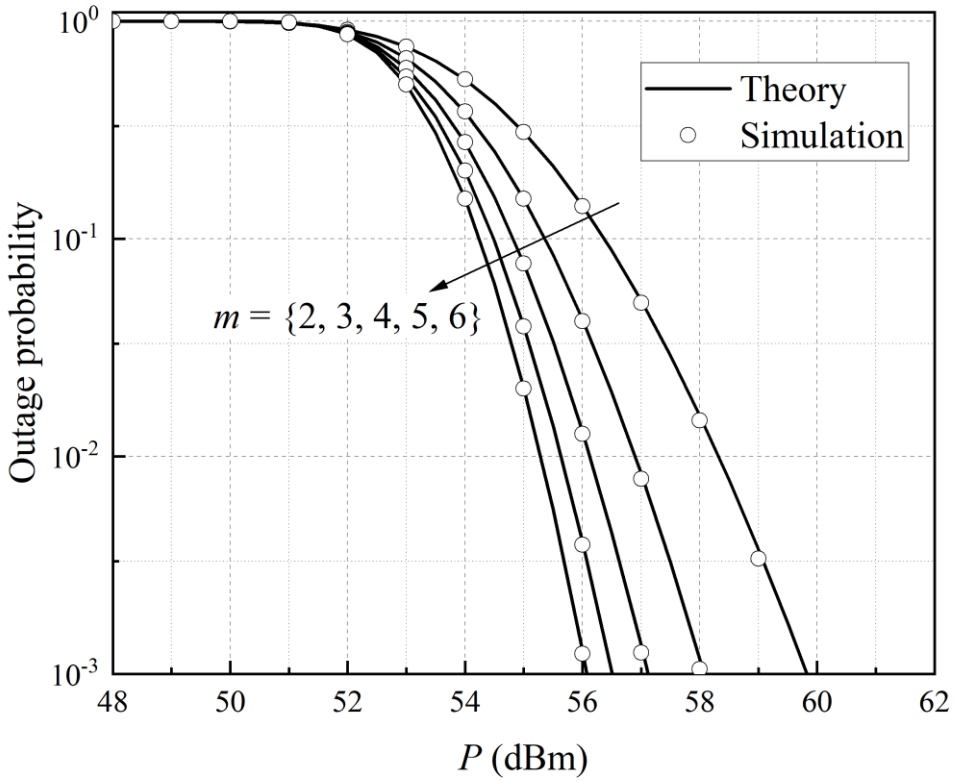

Figure 3.3: Outage probability for different m parameter.

3, 115 dBm transmitted power is needed to achieve OP of 10^{-3}. From the plots, it is shown that more transmit power is needed when $n = 3$, as opposed to when $n = 1$ and $n = 2$ to achieve the same OP. The reason for this is that as the number of RISs, n, between BS and user increases, the path loss is increased. Consequently, in order to prevent a disruption in the transmission of the message χ, a greater amount of power, P, must be allocated. The plots are maintained at a 40 dBm interval, which means that to add one more RIS to the system, 40 dBm more transmit power is needed to achieve the same OP. It is important to highlight that all the analytical results are in good agreement with the simulation results. In the plot, simulation results are given with the continuous curve, while analytical results are illustrated with the circles.

Figure 3.3 depicts the OP versus transmit power plots for cascaded RISs-aided system with two RISs. The OP is evaluated under different m parameter of the Nakagami-m distribution, where $m \in \{2, 3, 4, 5, 6\}$. In addition, each RIS is equipped with eight reflecting passive elements. For all plots, the spread parameter of Nakagami-m distribution is set to $\Omega = 1$. The OP of 10^{-3} is achieved between 56 dBm and 60 dBm for all values of m. As m parameter increases, the OP improves by using less power. This can be explained by the fact that as m parameter increase, it means that there are more paths between BS and user, consequently more power would be delivered. Also, in the plot, analytical results were validated by the simulation. The open circles fall on the continuous curves that prove the correction of analytical output.

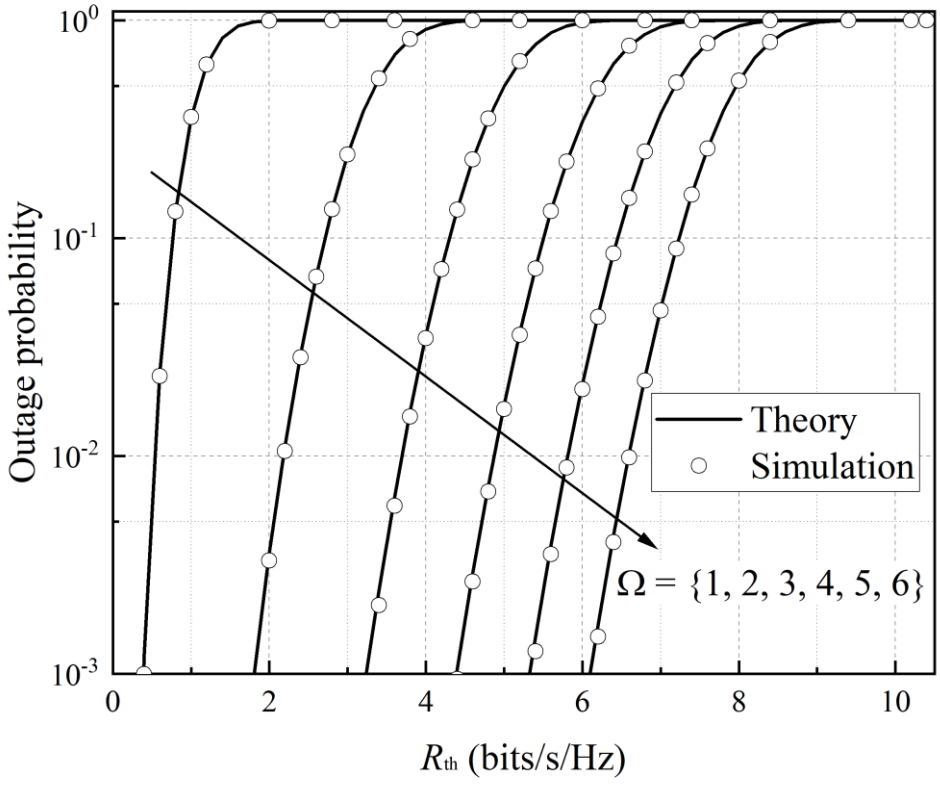

Figure 3.4: Outage probability versus rate threshold.

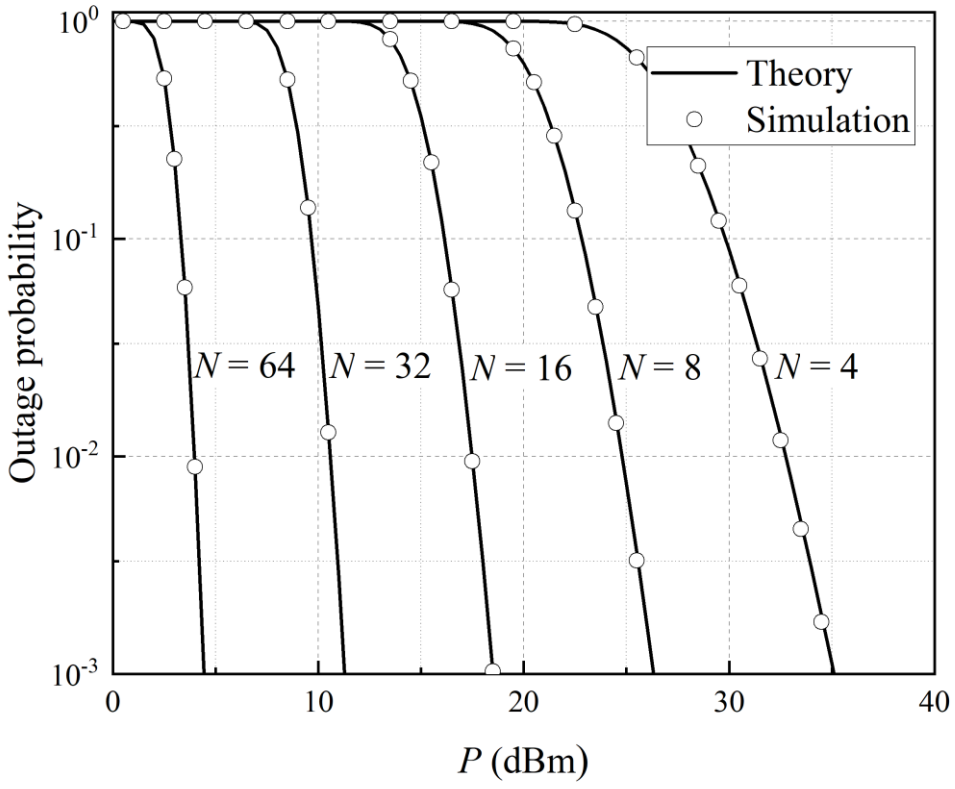

Figure 3.5: Outage probability analysis for different N parameter.

Figure 3.4 displays the the performance of cascaded RISs-aided system with two RISs, where each RIS has eight passive reflecting elements, in terms of OP versus rate threshold , R_{th}, for $\Omega \in \{1, 2, 3, 4, 5, 6\}$. The transmit power, P = 50 dBm, is kept constant for all cases. The m parameter of Nakagami-m distribution is set to m = 2. As we increase Ω parameter, the desired rate threshold is increased non-linearly to obtain the same OP. The results show that OP of 10^{-3} is achieved at $R_{\text{th}} \in \{0.5, 1.8, 3.2, 4.4, 5.2, 6.1\}$ bits/s/Hz for $\Omega \in \{1, 2, 3, 4, 5, 6\}$, respectively. This indicates that increasing the value of Ω results in improved OP. Indeed, Ω is responsible for the received average power. As we receive more power, it means less attentuation and better outage probability. Also, the plot shows that analytical and simulation results are in good agreement between each other.

Table 3.1: Obtained total errors for the results in Figures 3.2, 3.3, and 3.5.

Number of RIS, n	**Total error, Δ_n**	**Number of elements, N**	**Total error, Δ_N**	**Shape parameter, m**	**Total error, Δ_m**
1	$18.6*10^{-3}$	4	$17.1*10^{-3}$	2	$16.1*10^{-3}$
		8	$8.3*10^{-3}$	3	$11.7*10^{-3}$
2	$52.9*10^{-3}$	16	$4.4*10^{-3}$	4	$8.5*10^{-3}$
		32	$2.8*10^{-3}$	5	$5.8*10^{-3}$
3	$91.9*10^{-3}$	64	$2.5*10^{-3}$	6	$4.7*10^{-3}$

Figure 3.5 shows the performance of the single RIS-aided system evaluated in terms of OP metric versus transmit power P for different number of passive reflecting elements, $N \in \{4, 8, 16, 32, 64\}$. The shape and spread parameters of Nakagami-m distribution are set to $m = 2$ and $\Omega = 1$. It is clear from the figure that increasing the number of passive reflecting elements, N, results in an improvement in the overall performance of the OP. The reason for this is because the greater the number of passive components that are engaged in the reflection, the greater the number of signal replicas that are directed toward the destination, which ultimately results in the amplification gain. As a consequence, the transmission power that is required for data transfer may be reduced. The OP of 10^{-3} is achieved at P = {4, 11, 18, 26, 35} dBm for N = {4, 8, 16, 32, 64}, respectively, with approximately 8 dBm gap. The results suggest that if we use more passive elements in a single RIS, the same message can be transmitted with less power. For double increase of number of reflecting elements, we achieve 8 dBm decrease in the power. For all curves in the plot, analytical results well fits the simulation output.

Based on the acceptance of the premise that the probability density function (PDF) of RV Z follows the Gamma distribution, the KS goodness-of-fit test provides evidence that the approximation approach given in this work is correct. The total errors for the findings produced in Figures 3.2, 3.3, and 3.5 are computed and displayed in Table 3.1. This is done so that the validity of the approximation may be cross checked. According to the data shown in the table,

an increase in the value of *n* results in an increase in the overall approximation error. This is due to the fact that the number of RVs that need to be estimated is exactly proportional to the number of RISs that are present. When the value of *m* is increased, the approximation error decreases from 1.6×10^{-2} to 0.5×10^{-2}which is a significant drop. In addition, it is worth noting that the approximation errors reduce from 1.7×10^{-2} to 0.25×10^{-2} as the value of *N* increases. When the value of *n* is equal to three, the approximation error for *n* is the largest with a value of 9×10^{-2}. This is due to the fact that the correlation between RVs only becomes apparent when *n* is more than one, which necessitates extra approximation stages in order to collect the Gamma parameters. From the table, we can confirm that our approximation improves as we decrease *n* and *N*, and increase *m*.

3.2 RIS-partitioning system

This section presents analytical and experimental results and discussions for the RIS partiotining system.

3.2.1 Analytical approach

Both *X* and *Y* are well approximated by Gaussian and Gamma distributions, respectively. The corresponding parameters are defined by using MMM.

Figure 3.6 illustrates the distribution of *X* RV defined in eq. (2.25). The blue plot shows distribution of *X* obtained by using simulation, and red curve shows its corresponsing Gaussian approximation. The Gaussian distribution parameters are obtained using eqs. (2.27) and (2.28). From the plot, it is shown that simulational and analytical results well fits each other. Futher analysis can be done by using properties of Gaussian distribution.

Figure 3.7 shows distribution of *Y* RV defined in eq. (2.26). The blue plot shows distribution of *X* obtained by using simulation, and red curve shows its corresponsing Gamma approximation. The Gaamma distribution parameters are obtained using eqs. (2.31) and (2.32).

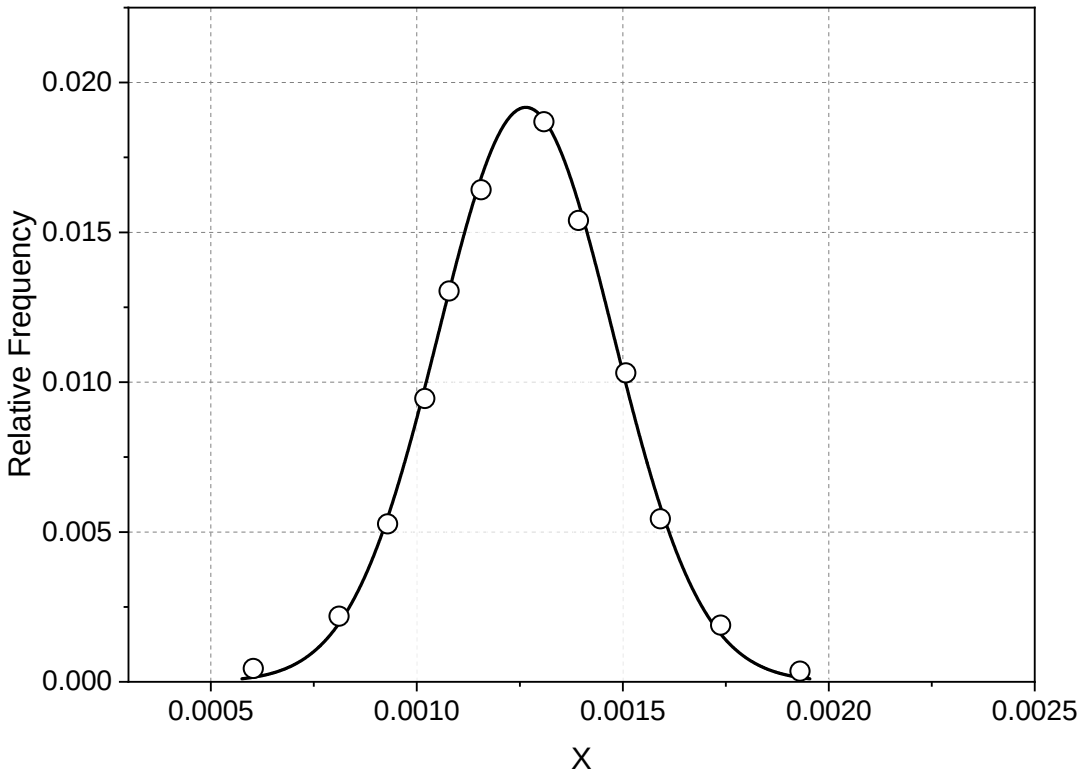

Figure 3.6: Distribution of X RV

From the plot, it is shown that simulational and analytical results well fits each other. Futher analysis can be done by using properties of Gamma distribution.

The PDF and OP for RIS partitioning system model is still under investigation. The correlation between *X* and *Y* makes the analysis of SINR very complex. To the best of authors knowledge, the distribution of ratio of corelated Gaussian and Gamma RVs has not been investigated in the literature, thus it is one of the challenges that has not been solved. However, it is our future reasearch direction to analyse the distribution of correlated RVs.

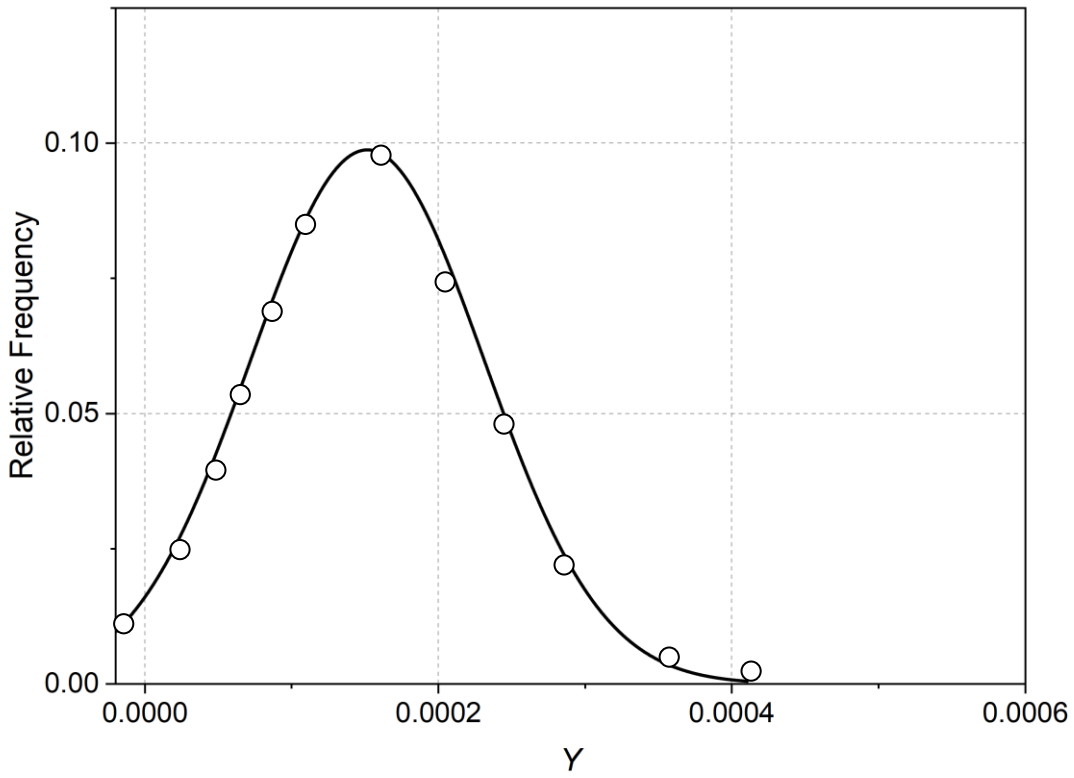

Figure 3.7: Distribution of Y RV

3.2.2 Experimental Approach

In this subsection, the results of the experiment are discussed for both near-field and far-field communications. For near-field communication, 8 cases are considered for different positions of two users.

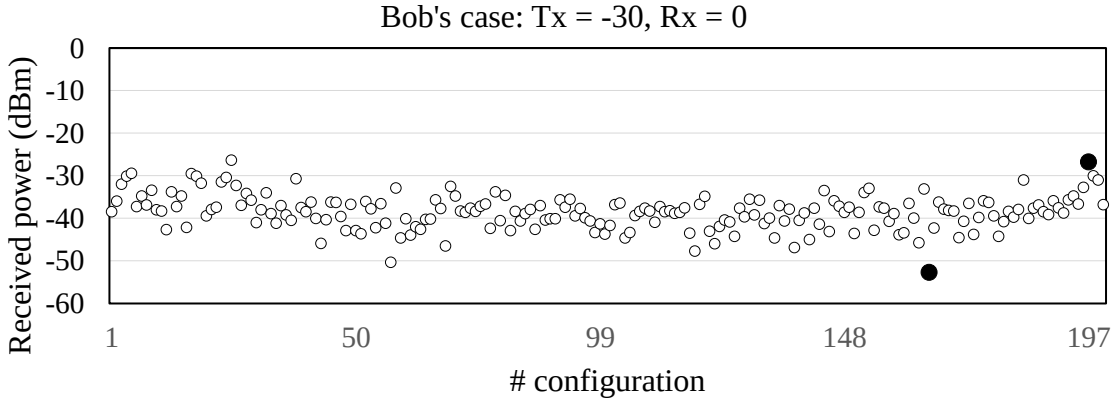

Figure 3.8: Received power for Bob positioned at 0°.

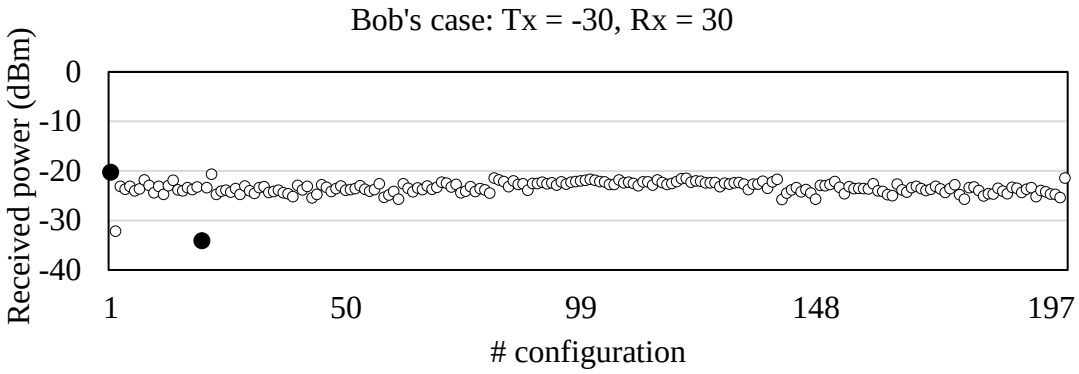

Figure 3.9: Received power for Bob positioned at 30°.

Figure 3.8 illustrates received power in dBm for each Bob's codebook when transmitter is located at (-30°) and Bob at 0°. The maximum power is -26.732 dBm and the corresponding codebook is 197. The difference between maximum and minimum received powers is 25.95 dBm. In average, most of the signals were received in the range of (-38.282, -35.882] dBm.

Figure 3.9 illustrates received power in dBm for each Bob's codebook when transmitter is located at (-30°) and Bob at 30°. The maximum power is -20.291 dBm and the corresponding codebook is 1. The difference between maximum and minimum received powers is 13.856 dBm. In average, most of the signals were received in the range of (-24.067, -23.227] dBm.

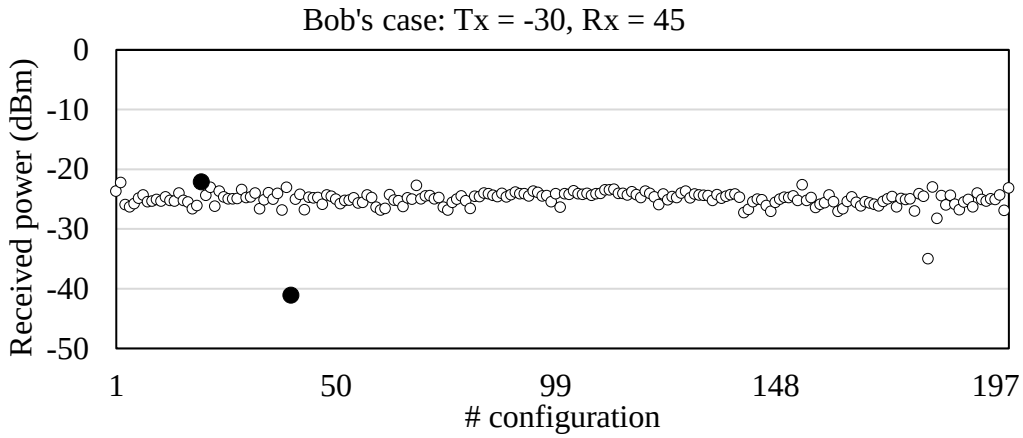

Figure 3.10: Received power for Bob positioned at 45°.

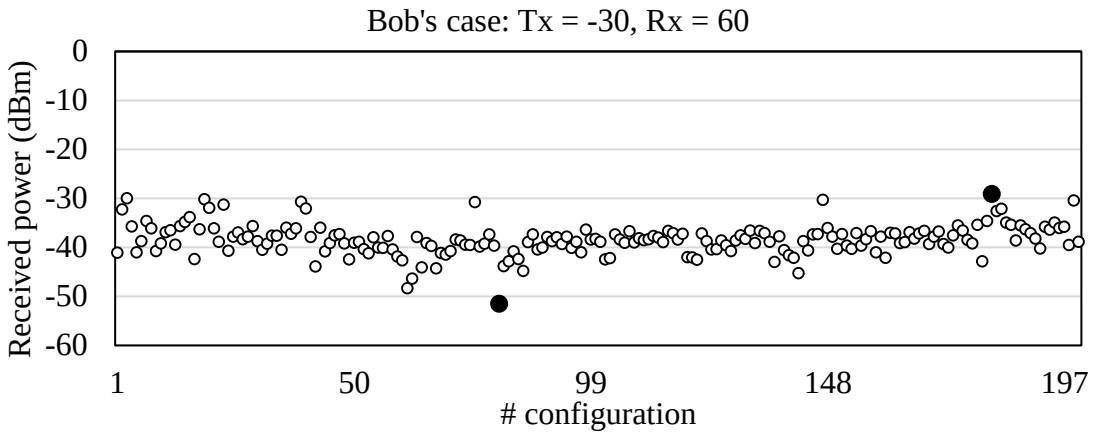

Figure 3.11: Received power for Bob positioned at 60°.

Figure 3.10 illustrates received power in dBm for each Bob's codebook when transmitter is located at (-30°) and Bob at 45°. The maximum power is -22.101 dBm and the corresponding codebook is 20. The difference between maximum and minimum received powers is 18.993 dBm. In average, most of the signals were received in the range of (-25.094, -23.094] dBm.

Figure 3.11 illustrates received power in dBm for each Bob's codebook when transmitter is located at (-30°) and Bob at 60°. The maximum power is -29.09 dBm and the corresponding codebook is 182. The difference between maximum and minimum received powers is 22.435 dBm. In average, most of the signals were received in the range of (-40.125, -38.225] dBm.

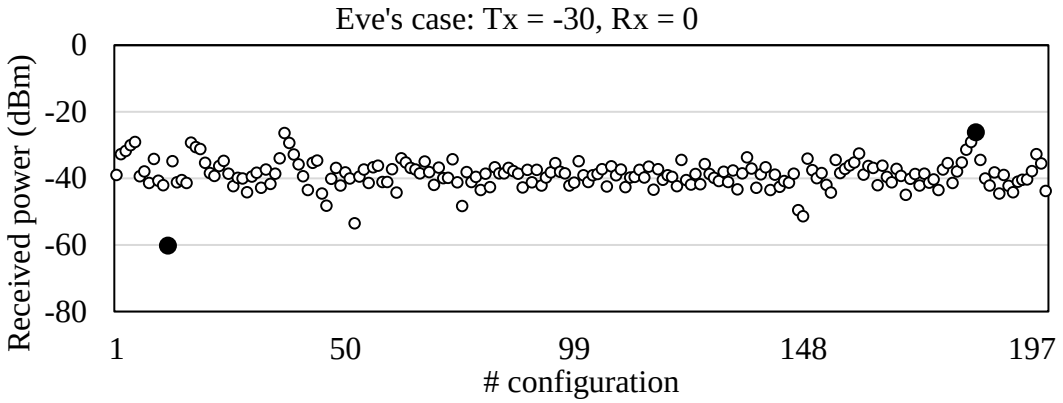

Figure 3.12: Received power for Eve positioned at 0°.

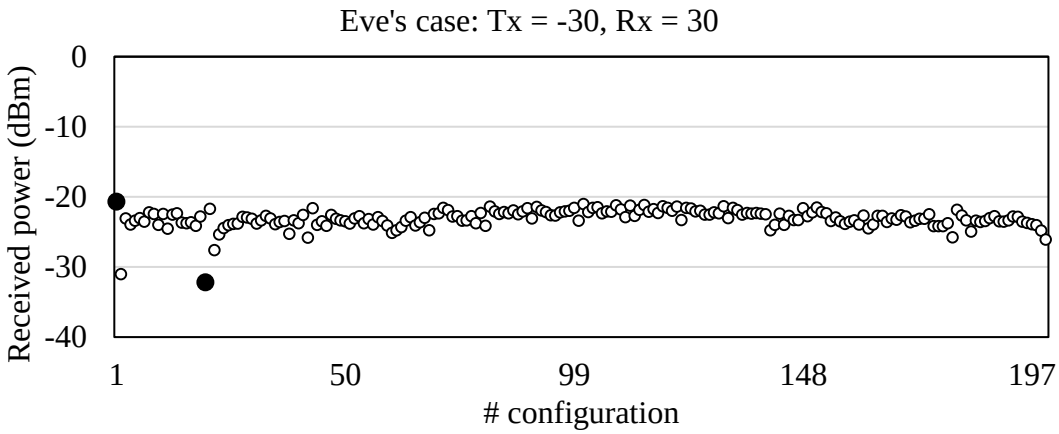

Figure 3.13: Received power for Eve positioned at 30°.

Figure 3.12 illustrates received power in dBm for each Eve's codebook when transmitter is located at (-30°) and Eve at 0°. The maximum power is -26.209 dBm and the corresponding codebook is 185. The difference between maximum and minimum received powers is 34.031 dBm. In average, most of the signals were received in the range of (-40.24, -37.74] dBm.

Figure 3.13 illustrates received power in dBm for each Eve's codebook when transmitter is located at (-30°) and Eve at 30°. The maximum power is -20.699 dBm and the corresponding codebook is 1. The difference between maximum and minimum received powers is 11.53 dBm. In average, most of the signals were received in the range of (-24.129, -23.319] dBm.

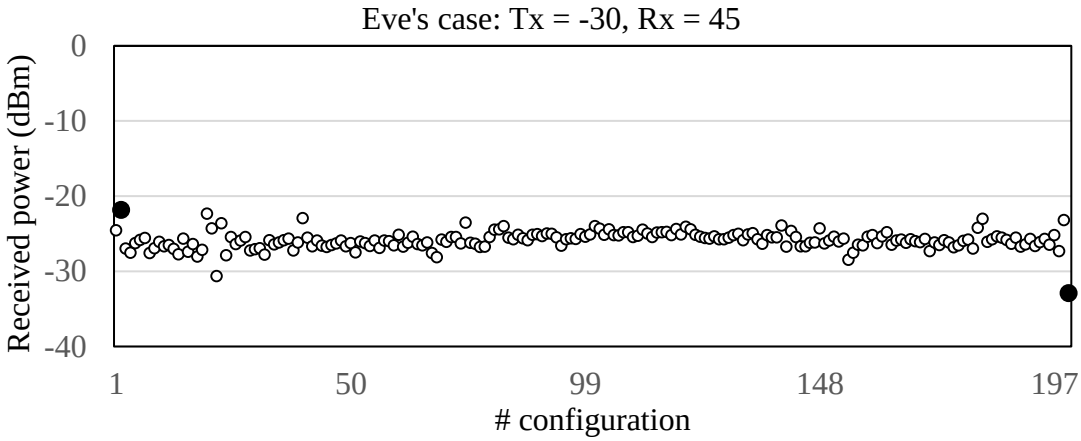

Figure 3.14: Received power for Eve positioned at 45°.

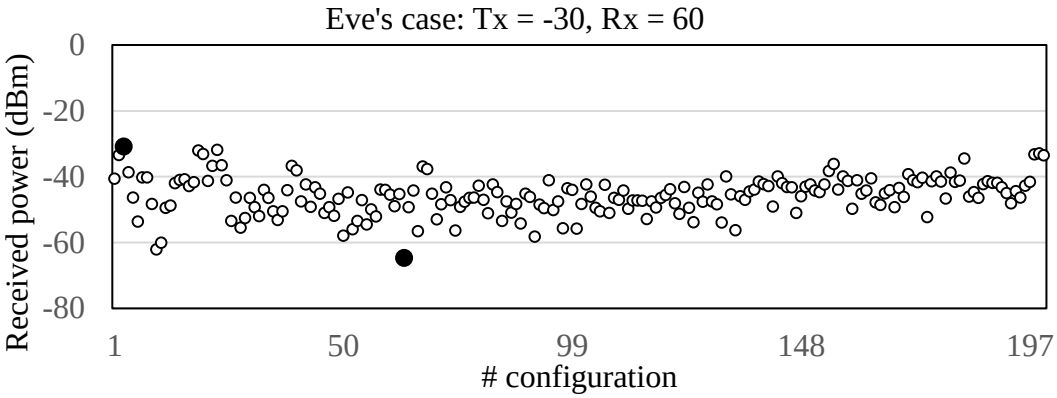

Figure 3.15: Received power for Eve positioned at 60°.

Figure 3.14 illustrates received power in dBm for each Eve's codebook when transmitter is located at (-30°) and Eve at 45°. The maximum power is -21.826 dBm and the corresponding codebook is 2. The difference between maximum and minimum received powers is 11.114 dBm. In average, most of the signals were received in the range of (-25.84, -25.13] dBm.

Figure 3.15 illustrates received power in dBm for each Eve's codebook when transmitter is located at (-30°) and Eve at 60°. The maximum power is -30.839 dBm and the corresponding codebook is 3. The difference between maximum and minimum received powers is 33.831 dBm. In average, most of the signals were received in the range of (-47.67, -44.27] dBm.

Table 3.2 illustrates best and worst received powers for four positions, namely 0°, 30°, 45°, and 60°, for both Bob and Eve. For all cases, transmitter position is fixed and located at -30°. The codebooks used bor Bob and Eve are different. Also, the table illustrates the corresponding codebook for the best and worst cases. From the comparison table, it is evident that the maximum power is achieved when both Bob and Eve is located at 30°. This achieved because RIS acts more as reflector instead of beamforming. The second best results for both receivers are achieved at the angle of 45°. When the receivers are situated at 0° and 60° degrees

Table 3.2: Comparison of received powers for Bob and Eve.

Bob's case	Eve's case
$T_x = -30°, R_x = 0°$	
Best: -26.338 dBm, Codebook: 197	**Best**: -26.209 dBm, Codebook: 185
Worst: -52.682 dBm, Codebook: 165	**Worst**: -60.240 dBm, Codebook: 12
$T_x = -30°, R_x = 30°$	
Best: -20.291 dBm, Codebook: 1	**Best**: -20.699 dBm, Codebook: 1
Worst: -34.144 dBm, Codebook: 20	**Worst**: -32.229 dBm, Codebook: 20
$T_x = -30°, R_x = 45°$	
Best: -22.101 dBm, Codebook: 20	**Best**: -21.826 dBm, Codebook: 2
Worst: -41.094 dBm, Codebook: 40	**Worst**: -32.940 dBm, Codebook: 200
$T_x = -30°, R_x = 60°$	
Best: -29.090 dBm, Codebook: 182	**Best**: -30.839 dBm, Codebook: 3
Worst: -51.525 dBm, Codebook: 80	**Worst**: -64.670 dBm, Codebook: 63

they receive less power. From these results we can say that if the receiver position is close to 30° then received power is higher.

Table 3.3 illustrates the received power when RIS partitioning were used. In this case, RIS is divided into two categories. Upper 200 elements of RIS is set with the best codebook of Bob and bottom 200 elements works with the best codebook of Eve. If Bob and Eve both are at 0° position then we obtain -20.948 dBm received power. It is almost 6 dBm higher than the case when Bob and Eve's codebooks were used alone. For the rest of positions, the received power is around -26 dBm.

Table 3.3: Received power when RIS partitioning is used

Bob and Eve positions	Received power
Bob's position is 0°, Codebook: 197 Eve's position is 0°, Codebook: 185	-20.948 dBm
Bob's position is 0°, Codebook: 197 Eve's position is 30°, Codebook: 1	-26.324 dBm
Bob's position is 0°, Codebook: 197 Eve's position is 45°, Codebook: 2	-27.587 dBm
Bob's position is 0°, Codebook: 197 Eve's position is 60°, Codebook: 3	-26.236 dBm

For the far-field communication, first far-field distance is calculated and the experiment has been performed on RIS partitioning.

The maximum received power when all 400 elements were involved was -65 dBm. There was 5 dBm more attenuation when half of the RIS elements were involved for beamforming while the rest of elements were turned off. The experiment was repeated for different transmitted powers to validate far-field communication. According to the theory, transmitter power and received power should be linearly dependent, thus for -6 dBm, -10 dBm, and -20 dBm transmitted powers we obtained -71 dBm, -75 dBm, and -85 dBm received powers, respectively. This linear relationship proved that the distance was selected properly for far-field communication.

Chapter 4 – Conclusion

This master thesis work investigated one of the technological enablers of 6G – RIS. The paper deeply explained architecture, working principles, and functionalities of RIS. Two system models were considered to evaluate the performance of the RIS–aided system. The first system model is cascaded RISs-aided system. For this system model, state of the art research was explained and gap in the research was identified. The use of many RISs in series is less investigated topic and considering one of the practical parameters, namely phase errors, has not been investigated in the literature. The work presents system analysis and evaluates the system performance in terms of OP metric. The results show that the derived analytical approximation well fits the simulation results. The approximation errors were validated by using KS goodness of fit test. The system evaluation outcomes conclude that increasing number of RISs in series decreases OP metric, because involvement of more RISs increases the path-loss of the system thus more power would be required. The increase of other parameters of the system, namely diversity path patameter, m, average received power parameter, Ω, and number of reflecting element per RIS, N, improves the OP metric. Increasing m parameter means that there is more path for the signal to reach the user, thus more power would be received to the destination. Average power parameter identifies received average power, more received power means better OP metric. Increasing number of reflecting elements is one of the important results, because each double increase of N increases the received power by 8 dBm. For all these results, both analytical and simulational outputs are presented. Approximation error is calculated for all the outcomes and they were validated by the KS goodness of fit test. The next system model is RIS partiotioning network. For this system both analytical and experimental analysis were performed. For the analytical results, the distribution of two RVs generated from the system model, namely X and Y, were approximated by Gaussian and Gamma distributions

by using MMM. The approximations were validated by using MATLAB's distribution fitting tool. Experimental results shows that RIS partiotioning works and has many advantages. For near-field communication, there is a 6 dBm improve on received power when both NOMA users are located at the same position. Also, having different positions for NOMA users do not deteriorate the received power instead shows the same results as all elements of RIS are used to serve only one user. For far-field communication, using half of the RIS elements showed only -5 dBm less received power as compared to the case when all the RIS elements were used. To conclude, both these system models showed perfromance analysis of RIS-aided systems and proves that utilization of RIS has great advantage on wireless networks.

Future research directions include analytical analysis of RIS-partitioning system, because closed-form expression for OP is still under research. In addition, the reflection properties (amplitude and phase) of RIS still ignored in many reserch works, therefore this topics need to be investigated in future research, because their effect to the system performance is still unclear.

List of Publication

[1] Z. Zhakipov, K. M. Rabie, X. Li and G. Nauryzbayev, "Accurate Approximation to Channel Distributions of Cascaded RIS-Aided Systems With Phase Errors Over Nakagami-m Channels," in IEEE Wireless Communications Letters, vol. 12, no. 5, pp. 922-926, May 2023, doi: 10.1109/LWC.2023.3251647.

Bibliography

[1] I. F. Akyildiz, A. Kak, and S. Nie, "6G and beyond: The future of wireless communications systems," *IEEE Access*, vol. 8, pp. 133 995–134 030, 2020. DOI: 10.1109/ACCESS.2020.3010896.

[2] W. Jiang et al., "The road towards 6G: A comprehensive survey," *IEEE Open Journal of the Communications Society*, vol. 2, pp. 334–366, 2021. DOI: 10.1109/OJCOMS.2021.3057679.

[3] Q. Wu and R. Zhang, "Towards smart and reconfigurable environment: Intelligent reflecting surface aided wireless network," *IEEE Communications Magazine*, vol. 58, no. 1, pp. 106–112, 2020. DOI: 10.1109/MCOM.001.1900107.

[4] C. Liaskos, S. Nie, A. Tsioliaridou, A. Pitsillides, S. Ioannidis, and I.Akyildiz, "A new wireless communication paradigm through software-controlled metasurfaces," *IEEE Communications Magazine*, vol. 56, no. 9, pp. 162–169, 2018. DOI: 10.1109/MCOM.2018.1700659.

[5] H. Yang, X. Chen, F. Yang, et al., "Design of resistor-loaded reflectarray elements for both amplitude and phase control," *IEEE Antennas and Wireless Propagation Letters*, vol. 16, pp. 1159–1162, 2017. DOI: 10.1109/LAWP.2016.2626318.

[6] Q. Wu and R. Zhang, "Beamforming optimization for intelligent reflecting surface with discrete phase shifts," in *ICASSP 2019 - 2019 IEEE International Conference on Acoustics, Speech and Signal Processing (ICASSP)*, 2019, pp. 7830–7833. DOI: 10.1109/ICASSP.2019.8683145.

[7] L. Lu, G. Y. Li, A. L. Swindlehurst, A. Ashikhmin, and R. Zhang, "An overview of massive MIMO: Benefits and challenges," *IEEE Journal of Selected Topics in Signal Processing*, vol. 8, no. 5, pp. 742–758, 2014. DOI:10.1109/JSTSP.2014.2317671.

[8] A. Papazafeiropoulos et al., "Intelligent reflecting surface-assisted MU-MISO systems with imperfect hardware: Channel estimation and beamforming design," *IEEE Transactions on Wireless Communications*, vol. 21,no. 3, pp. 2077–2092, 2022. DOI: 10.1109/TWC.2021.3109391.

[9] T. Van Chien et al., "Reconfigurable intelligent surface-assisted cell-free massive MIMO systems over spatially-correlated channels," *IEEE Transactions on Wireless Communications*, vol. 21, no. 7, pp. 5106–5128, 2022. DOI: 10.1109/TWC.2021.3136925.

[10] J. Xu and Y. Lin, "A novel channel model for reconfigurable intelligent surface-assisted wireless networks," in *GLOBECOM 2020 – 2020 IEEE Global Communications Conference*, 2020, pp. 01–06. DOI: 10.1109/GLOBECOM42002.2020.9322278.

[11] V.-D. Phan et al., "Performance of cooperative communication system with multiple reconfigurable intelligent surfaces over Nakagami-m fading channels," *IEEE Access*, vol. 10, pp. 9806–9816, 2022. DOI: 10.1109/ACCESS.2022.3144364.

[12] M. A. ElMossallamy, H. Zhang, L. Song, K. G. Seddik, Z. Han and G. Y. Li, "Reconfigurable Intelligent Surfaces for Wireless Communications: Principles, Challenges, and Opportunities," in *IEEE Transactions on Cognitive Communications and Networking*, vol. 6, no. 3, pp. 990-1002, Sept. 2020, doi: 10.1109/TCCN.2020.2992604.

[13] E. Basar, M. Di Renzo, J. De Rosny, M. Debbah, M. -S. Alouini and R. Zhang, "Wireless Communications Through Reconfigurable Intelligent Surfaces," in *IEEE Access*, vol. 7, pp. 116753-116773, 2019, doi: 10.1109/ACCESS.2019.2935192.

[14] Q. Wu, S. Zhang, B. Zheng, C. You and R. Zhang, "Intelligent Reflecting Surface-Aided Wireless Communications: A Tutorial," in *IEEE Transactions on Communications*, vol. 69, no. 5, pp. 3313-3351, May 2021, doi: 10.1109/TCOMM.2021.3051897.

[15] L. Yang, F. Meng, Q. Wu, D. B. da Costa and M. -S. Alouini, "Accurate Closed-Form Approximations to Channel Distributions of RIS-Aided Wireless Systems," in *IEEE Wireless Communications Letters*, vol. 9, no. 11, pp. 1985-1989, Nov. 2020, doi: 10.1109/LWC.2020.3010512.

[16] H. Zhang, B. Di, L. Song and Z. Han, "Reconfigurable Intelligent Surfaces Assisted Communications With Limited Phase Shifts: How Many Phase Shifts Are Enough?," in *IEEE Transactions on Vehicular Technology*, vol. 69, no. 4, pp. 4498-4502, April 2020, doi: 10.1109/TVT.2020.2973073.

[17] F. A. P. de Figueiredo et al., "Large Intelligent Surfaces With Discrete Set of Phase-Shifts Communicating Through Double-Rayleigh Fading Channels," in *IEEE Access*, vol. 9, pp. 20768-20787, 2021, doi: 10.1109/ACCESS.2021.3053773.

[18] Y. Zhang, J. Zhang, M. D. Renzo, H. Xiao and B. Ai, "Performance Analysis of RIS-Aided Systems With Practical Phase Shift and Amplitude Response," in *IEEE Transactions on Vehicular Technology*, vol. 70, no. 5, pp. 4501-4511, May 2021, doi: 10.1109/TVT.2021.3069174.

[19] P. Xu, W. Niu, G. Chen, Y. Li and Y. Li, "Performance Analysis of RIS-Assisted Systems With Statistical Channel State Information," in *IEEE Transactions on Vehicular Technology*, vol. 71, no. 1, pp. 1089-1094, Jan. 2022, doi: 10.1109/TVT.2021.3126374.

[20] D. Tyrovolas, S. A. Tegos, E. C. Dimitriadou-Panidou, P. D. Diamantoulakis, C. K. Liaskos and G. K. Karagiannidis, "Performance Analysis of Cascaded Reconfigurable Intelligent Surface Networks," in *IEEE Wireless Communications Letters*, vol. 11, no. 9, pp. 1855-1859, Sept. 2022, doi: 10.1109/LWC.2022.3184635.

[21] W. Mei and R. Zhang, "Cooperative Beam Routing for Multi-IRS Aided Communication," in *IEEE Wireless Communications Letters*, vol. 10, no. 2, pp. 426-430, Feb. 2021, doi: 10.1109/LWC.2020.3034370.

[22] Y. Han, S. Zhang, L. Duan and R. Zhang, "Cooperative Double-IRS Aided Communication: Beamforming Design and Power Scaling," in *IEEE Wireless Communications Letters*, vol. 9, no. 8, pp. 1206-1210, Aug. 2020, doi: 10.1109/LWC.2020.2986290.

[23] M. Makin et al., “Optimal RIS partitioning and power control for bidirectional NOMA networks,” *IEEE Transactions on Wireless Communications*, pp. 1–1, 2023. DOI: 10.1109/TWC.2023.3306048.

[24] Z. Yang, Y. Liu, Y. Chen and N. Al-Dhahir, "Machine Learning for User Partitioning and Phase Shifters Design in RIS-Aided NOMA Networks," in *IEEE Transactions on Communications*, vol. 69, no. 11, pp. 7414-7428, Nov. 2021, doi: 10.1109/TCOMM.2021.3100866.

[25] A. Khaleel and E. Basar, "A Novel NOMA Solution With RIS Partitioning," in *IEEE Journal of Selected Topics in Signal Processing*, vol. 16, no. 1, pp. 70-81, Jan. 2022, doi: 10.1109/JSTSP.2021.3127725.

[26] R. A. Tasci, F. Kilinc, A. Celik, A. Abdallah, A. M. Eltawil and E. Basar, "RIS-Assisted Grant-Free NOMA," *ICC 2023 - IEEE International Conference on Communications, Rome, Italy*, 2023, pp. 4323-4328, doi: 10.1109/ICC45041.2023.10278893.

[27] E. Arslan et al., "Reconfigurable Intelligent Surface Enabled Over-the-Air Uplink NOMA," in *IEEE Transactions on Green Communications and Networking*, vol. 7, no. 2, pp. 814-826, June 2023, doi: 10.1109/TGCN.2022.3227870.

[28] C. Huang, R. Mo, and C. Yuen, “Reconfigurable intelligent surface assisted multiuser MISO systems exploiting deep reinforcement learning,” *IEEE Journal on Selected Areas in Communications*, vol. 38, no. 8, pp. 1839–1850, 2020. DOI: 10.1109/JSAC.2020.3000835.

[29] J. Gao et al., “Unsupervised learning for passive beamforming,” *IEEE Communications Letters*, vol. 24, no. 5, pp. 1052–1056, 2020. DOI: 10.1109/LCOMM.2020.2965532.

[30] H. Song et al., “Unsupervised learning-based joint active and passive beamforming design for reconfigurable intelligent surfaces aided wireless networks,” *IEEE Communications Letters*, vol. 25, no. 3, pp. 892–896, 2021. DOI: 10.1109/LCOMM.2020.3041510.

[31] A. Taha, M. Alrabeiah, and A. Alkhateeb, “Enabling large intelligent surfaces with compressive sensing and deep learning,” *IEEE Access*, vol. 9, pp. 44 304–44 321, 2021. DOI: 10.1109/ACCESS.2021.3064073.

[32] I. S. Gradshteyn and I. M. Ryzhik, *Table of Integrals, Series, and Products; 7th edition*. Academic Press, May 2014.

[33] L. Kong et al., “Effective rate evaluation of RIS-assisted communications using the sums of cascaded $\alpha - \mu$ random variates,” *IEEE Access*, vol. 9, pp. 5832–5844, Jan. 2021. DOI: 10.1109/ACCESS.2020.3048882.

[34] Z. Zhakipov, K. M. Rabie, X. Li and G. Nauryzbayev, "Accurate Approximation to Channel Distributions of Cascaded RIS-Aided Systems With Phase Errors Over Nakagami-m Channels," in IEEE Wireless Communications Letters, vol. 12, no. 5, pp. 922-926, May 2023, doi: 10.1109/LWC.2023.3251647.